

RESEARCH

Open Access



# Discovery of novel *Trichoderma*-based bioactive compounds for controlling potato virus Y based on molecular docking and molecular dynamics simulation techniques

Mohamed N. Rizk<sup>1\*</sup>, Hammad A. Ketta<sup>2</sup> and Yasser M. Shabana<sup>1,3</sup>

## Abstract

**Background** Although potato virus Y (PVY) is the most serious virus-infecting potato plants worldwide, the losses concurred by it remain unmanageable due to the lack of efficient anti-PVY agents. Hence, the objective of this study was to assess the antiviral properties of secondary metabolite compounds obtained from culture filtrates of four *Trichoderma* spp. isolates. The assessment was conducted using computational methods, including molecular docking, absorption, distribution, metabolism, excretion, and toxicity (ADMET) analysis, as well as molecular dynamics simulations. The aim was to develop novel and effective agents for combating PVY.

**Results** The GC–MS analysis of the studied *Trichoderma* spp. secondary metabolites revealed 24 compounds with relative amounts exceeding 10%. Molecular docking was then performed using MOE software to evaluate the activity of these compounds against the PVY protein coat (PDB-ID: 6HXX). Ningnanmycin and ribavirin, known plant virus inhibitors, were employed as reference ligands for comparison. Among the compounds tested, C9, C10, C13, and C19 exhibited superior docking scores, root mean square deviation (RMSD) values, and binding modes compared to the reference ligands. In addition, these compounds successfully passed the ADMET analysis. Further investigation focused on compounds C13 and C19, which underwent in-depth analysis through MDs for 100 ns. The MDs trajectories demonstrated that both complexes exhibited favorable stability, compactness, and binding modes throughout the simulation period. However, the C19/PVY-CP complex outperformed the C13 complex in all calculated parameters such as RMSD, root mean square fluctuation (RMSF), radius of gyration (RoG), solvent-accessible surface area (SASA), and intermolecular hydrogen bonds. Interestingly, these findings aligned with the results obtained from the docking analysis, indicating that C9 and C10 possess high potential against PVY, as they exhibited binding modes like that of C19.

**Conclusion** These promising outcomes provide a solid foundation for considering the potential use of compounds C9, C10, C13, and C19 as antiviral agents. Further experimental validation and in-depth studies are warranted to assess the efficacy and safety of these compounds and their potential as antiviral therapeutics. To our knowledge, this is the first report to study the biological activities of the *Trichoderma*-based bioactive compounds against PVY using computational techniques.

**Keywords** PVY, Coat protein, Antiviral, *Trichoderma*, GC–MS, *In silico*, Molecular docking, Molecular dynamic simulations

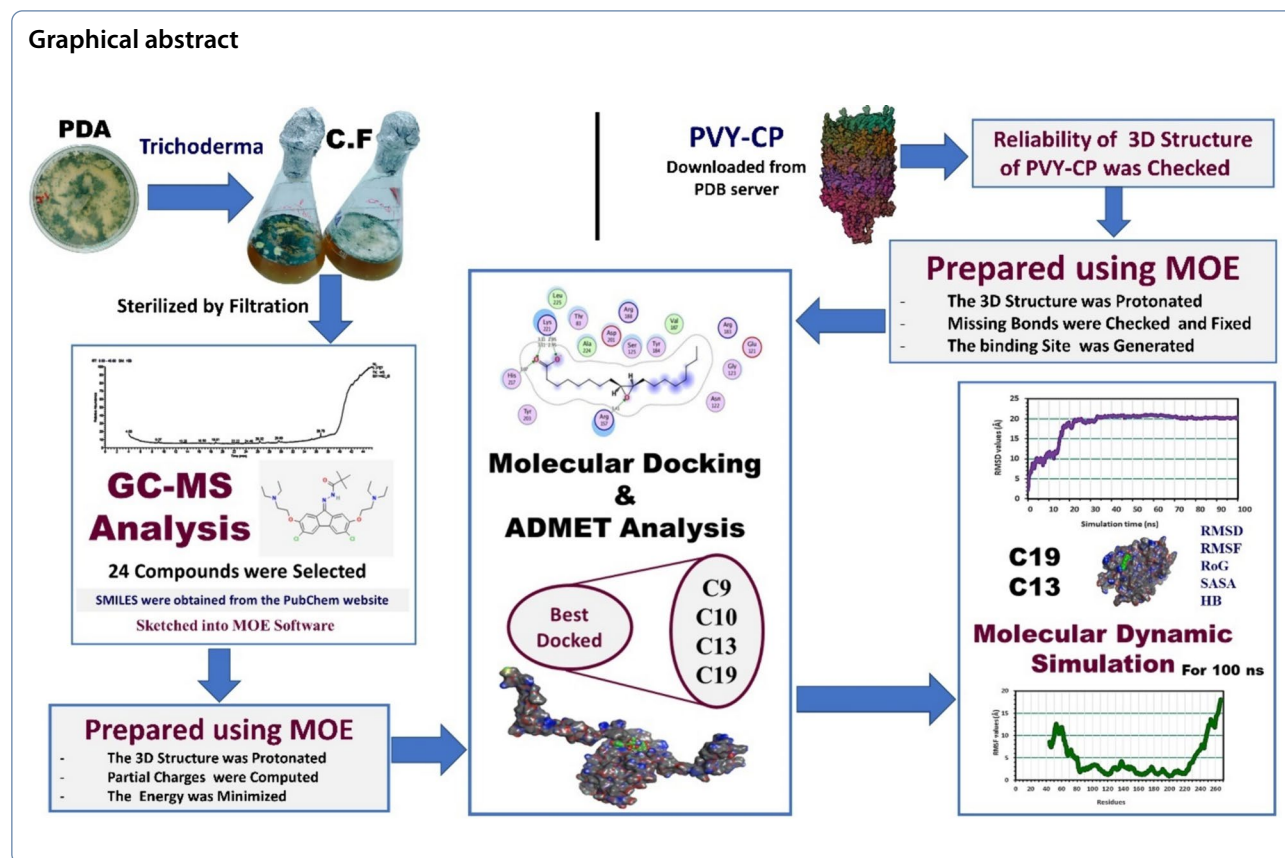
\*Correspondence:

Mohamed N. Rizk  
nasser@mans.edu.eg

Full list of author information is available at the end of the article



© The Author(s) 2024. **Open Access** This article is licensed under a Creative Commons Attribution 4.0 International License, which permits use, sharing, adaptation, distribution and reproduction in any medium or format, as long as you give appropriate credit to the original author(s) and the source, provide a link to the Creative Commons licence, and indicate if changes were made. The images or other third party material in this article are included in the article's Creative Commons licence, unless indicated otherwise in a credit line to the material. If material is not included in the article's Creative Commons licence and your intended use is not permitted by statutory regulation or exceeds the permitted use, you will need to obtain permission directly from the copyright holder. To view a copy of this licence, visit <http://creativecommons.org/licenses/by/4.0/>. The Creative Commons Public Domain Dedication waiver (<http://creativecommons.org/publicdomain/zero/1.0/>) applies to the data made available in this article, unless otherwise stated in a credit line to the data.



## Background

The potato plant (*Solanum tuberosum* L.), a member of the *Solanaceae* family, is the world's fourth most important food crop after rice, wheat, and maize. It is a highly nutritious and absorbable food. It contains carbohydrates, proteins, minerals, and vitamins [1]. According to a study by Myers et al. [2], 1.9–2.3 billion people obtain 60 to 70% of their iron and zinc requirements from potatoes. Elshahar et al. [3] reported that Egypt exported about 734,000 tons of potatoes in 2021, making it the sixth largest potato exporting country according to the statistical database (November 2021) of the Food and Agriculture Organization (FAO). Despite the fact that there are more than 50 plant viruses and one viroid that infect potato plants worldwide, only a few, including potato virus Y (PVY), have caused economic losses in potato yield [4]. PVY ranks as the fifth of the top ten economically important plant viruses, and it is also the most important one infecting potato plants wherever they are planted [5]. It causes many symptoms on potato plants and other solanaceous crops, such as veinal and stem necrosis, necrotic lesions, mild and severe mosaic, stunting, tuber ring spots, and leaf deformation, and can significantly reduce crop yield by up to 70% [6]. PVY

is a member of the genus *Potyvirus*, which belongs to the family *Potyviridae*. It exists as a set of strains that evolved by recombining mutations, which gives them a higher potential for adaptation to new potato cultivars. PVY is transmitted from infected plants to healthy ones mechanically by infective sap, vegetatively through tubers, and vectorially by aphids in non-persistent mode [6]. The genome of PVY is a 9.7 kilobase positive-sense single-stranded RNA (ssRNA) that encodes a single large polyprotein and is organized into ten mature proteins by specific viral proteases [7]. In addition, the overlapping coding region produces the important protein P3N-PIPO [8]. Potyviral proteins are characterized by performing several functions, such as virion uncoating, translation, reproduction, inhibition of host defenses, movement, and virion assembly. The coat protein (CP) of the potyvirus is recruited in more than 2000 copies to form the capsid protein around the viral genome in the later stages of infection, so it is responsible for giving the flexuous filament shape to virus particles [7]. Furthermore, the capsid protein of potyviruses is a multitasking protein that plays many roles, including regulation of the genome replication, involvement in viral transmission by aphids, cell-to-cell movement, and protection of the viral genome from

degradation, illustrating the importance of this protein during the viral infection cycle [9, 10].

Currently, managing plant virus infections is considered the most difficult challenge facing the agricultural sector in the world [11]. The development and application of effective antiviral agents to protect plants against viral infection has made some progress. For instance, the application of zinc oxide nanoparticles has shown good protective effects on tomato plants against infection caused by the tomato mosaic virus [12]. Also, the use of both melatonin and salicylic acid as antiviral compounds against alfalfa mosaic virus infecting eggplants showed convincing results without adverse effects on plants or the environment [13]. In addition, the use of oseltamivir and ribavirin compounds on potato plants to combat the disease caused by PVY achieved an effective impact on virus concentration and improved plant growth [14].

*Trichoderma* species are effective biocontrol agents of agricultural pests because of their rapid growth, high competition, and resistance to many toxic chemicals. They also promote plant growth and stimulate plant defense responses against diseases, insect damage, and abiotic stresses [15, 16]. In addition to their effectiveness against fungal diseases [17], *Trichoderma* species and/or their secondary metabolites have achieved promising findings in the management of plant diseases caused by bacteria [18] and viruses [19].

Using computational molecular modeling to simulate nature is one of the most important and cutting-edge approaches to examine the activities of a particular molecule. To study the behavior of a molecule at the binding sites of the three-dimensional structure of the target protein, several computational tools are employed. These techniques use physics-based equations to predict the interactions between the tested compounds and the target binding pocket by calculating the binding affinities of the considered complexes [4]. The aim of molecular docking studies is to determine how a molecule fits itself (a ligand) into another molecule (a protein) to understand its biological activities by looking at how it interacts with the target protein using scoring functions to determine which structure is most likely to exist in nature [20]. The docking analysis operates in two main phases: predicting the conformation/orientation, and position of the ligand in the target binding pocket (often referred to as pose), and calculating the binding affinities [21]. The results of molecular docking of arylidene dihydropyrimidine hydrazone derivatives against TMV coat protein showed that some of these chemicals are efficient against plant viral infection, suggesting that they might be potent antiviral agents in the pesticide market [23]. Previous docking studies by Nagalakshamma et al. [24], Abd-Alla et al. [25], and Omar et al. [23] showed good

agreement with experimental studies. Docking scores, root mean square distance (RMSD) values, and binding modes are used as criteria for valid docking analysis. The ligand effectively binds to the target receptor when its energy score is close to the reference one and its RMSD is close to 2 Å [26]. When a small molecule (a ligand) is delivered into the body of a living organism, its fate in the body is determined by a set of pharmacokinetic features known as ADMET which is the abbreviation of absorption, distribution, metabolism, excretion, and toxicity [27]. So, the evaluation of these parameters using computational tools is very important to ensure the safety of studied molecules on humans at early stages of drug development to save effort, time, and cost [28]. MDs are commonly used in combination with molecular docking to achieve more precise results. It is a computational technique used to understand the chemical interactions between atoms in a biomolecular system by applying Newton's equation of motion to calculate the velocity and location of each atom in the system under consideration throughout the MDS period [29].

The main objective of this study is to explore and evaluate the potential of the components derived from culture filtrates of *Trichoderma* isolates as anti-plant viral agents by computational techniques, including molecular docking, ADMET analysis, and molecular dynamic simulations. Several compounds that could directly hinder viral infection by targeting crucial components of the virus were identified.

## Materials and methods

### Source of *Trichoderma* isolates

In this study, four isolates (T1, T2, T3, and T4) of *Trichoderma* spp. were used in this study. These isolates were previously characterized and identified in an unpublished work and can be described as follows: T1 = *Trichoderma asperellum* isolate Ketta (accession no: PP228382); T2 = *T. asperellum* isolate RIZK24T2 (accession no: PP228383); T3 = *Trichoderma* sp.; T4 = *T. asperelloides* isolate RIZK24T4 (accession no: PP228384).

### *Trichoderma* culture filtrates (TCFs) preparation

*Trichoderma* isolates were cultured for 7 days on potato dextrose agar (PDA) medium at  $28 \pm 2$  °C. Two discs (5 mm-diameter) were taken from the peripheries of the colonies and transferred to conical flasks (500 ml) containing 250 ml of sterile potato dextrose broth (PDB) and incubated at  $28 \pm 2$  °C for 15 days without shaking. The crude culture filtrates were separated from the fungal mycelia by filtering them through three layers of filter paper (Whatman No. 1). To sterilize the filtrates,

Micro-POR Minigen Syringe Filters (Sterile NYLON, 25 mm/0.2 µm, Genetix Biotech Asia Pvt. Ltd) were used.

#### Effect of *Trichoderma* culture filtrates on the development of PVY symptoms

To investigate the impact of *Trichoderma* culture filtrates (TCFs) on the development of PVY symptoms, a foliar spray application was performed on potato plants twice: once 24 h before virus inoculation and then again 7 days after virus inoculation. The TCFs were applied using a hand-held low-pressure sprayer until drop-off [30], and the solutions contained 1% Tween-20. PVY isolate EGY\_RIZK24 (accession no. PP375808) was used for mechanical inoculation of the potato plants, following the procedure outlined in the previous study by Rizk et al. [14]. The emergence of PVY symptoms on the potato plants was assessed 21 days post-PVY inoculation.

#### Gas chromatography–mass spectrometry (GC–MS) analysis

For GC–MS analysis, freshly ten milliliters of sterilized culture filtrate of each isolate was used. In brief, the process involved using a direct capillary column (30 m × 0.25 mm × 0.25 µm film thickness) with a Trace GC-TSQ mass spectrometer (Thermo Scientific, Austin, TX, USA) to identify the chemical composition of the samples. The temperature of the column oven was initially maintained at 50 °C, and then it was raised by 5 °C/min to 250 °C and kept there for 2 min, before being raised by 30 °C/min to its ultimate temperature of 300 °C and held there for 2 min. Helium was employed as a carrier gas at a constant flow rate of 1 ml/min, while the injector and MS transfer line temperatures were maintained at 270 and 260 °C, respectively. The autosampler AS1300 combined with GC in split mode automatically injected diluted samples of 1 µl with a 4-min solvent delay. In full scan mode, EI mass spectra over the *m/z* range of 50–650 were collected at ionization voltages of 70 eV. The temperature of the ion source was fixed at 200 °C. The components were identified by comparing their mass spectra to those of the WILEY 09 and NIST 14 mass spectral databases [31].

#### Molecular docking studies

The molecular docking process was conducted in three phases: (1) preparation of the target receptor, (2) ligand preparation, and (3) docking run and findings analysis [32]. In the current investigation, docking experiments were carried out using the Molecular Operating Environment (MOE) software version 2015.10 (accessible online at <https://www.chemcomp.com/>) by applying the Amber10 EHT forcefield [22] to assess the effectiveness of *Trichoderma* spp. culture filtrates components against

potato virus Y (PVY). The potyvirus coat protein (CP) is responsible for the protection of the viral RNA from degradation enzymes, assembly of the virion, cell-to-cell movement, and vector-mediated transmission from host to host during the infection cycle of potyvirus species, including PVY [10]. Due to the importance of coat protein, it was chosen for designing and developing new anti-PVY agents.

#### Refinement and preparation of PVY protein coat structure

The X-ray pattern of unliganded PVY protein coat (ID: 6HXX) [33] was obtained from the Protein Data Bank (PDB) server of the Research Collaboratory for Structural Bioinformatics (RCSB; <http://www.rcsb.org/>). Some atoms, side chains, or even whole residues may be missed during the X-ray diffraction for the three-dimensional structure of proteins. These factors could interfere with the molecular docking procedure and affect the accuracy of the results. Therefore, refinement of the protein structure is necessary before running a docking process.

The “Build/check/repair model” option at the WHAT IF server (<https://swift.cmbi.umcn.nl/servers/html/>) was used to refine the 3D structure of the 6HXX protein. It is a common and essential step for obtaining accurate docking results [32]. The same protocols described by Shoala et al. [4] and Abdulhassan et al. [22] were followed throughout all of the processes for preparing the validated structure of the PVY protein coat for docking experiments. Briefly, using all default program elements, chain A of 6HXX was selected, and the protonate 3D of the protein was done (assigning ionization states and position hydrogens for a molecular system). Automated connection and typing were used to check the missing bonds of the atoms and fix them using the potential of the protein and its atoms option. Using the Site Finder option, the binding site was generated by choosing the largest pocket of the receptor, and dummy atoms were added to it. Finally, the biggest pocket was saved as a .moe extension file in the directory work for running docking.

#### Preparation of the tested compounds

Using SMILES (Simplified Molecular Input Line Entry System) that were obtained from the PubChem website (<https://pubchem.ncbi.nlm.nih.gov/>), all compounds under investigation were sketched into MOE program and then prepared using the protocol described by Al-Karmalawy et al. [34], which involved several steps: first, each compound was individually subjected to 3D protonation and partial charge calculations. Subsequently, energy minimization was performed until a 0.01 gradient was achieved. Afterward, each compound was saved as an .moe extension file in the designated “work” directory.

Finally, all prepared compounds were consolidated into a single database and exported as an .mdb file in the “work” directory for utilization in the docking experiment.

#### **Docking the target compounds to the binding pocket of PVY coat protein**

The docking of the target compounds to the binding pocket of the PVY coat protein was carried out following the protocol outlined by Shoala et al. [4]. The process is described below:

First, the pre-prepared target compounds, which were saved as a single MDB database, were docked into the binding pocket of the pre-prepared PVY protein coat, saved as an .moe file. The .moe file containing the protein coat was loaded into the MOE program, and the docking process was initiated through the Dock Panel. The general docking option was selected. In the system section of Dock Panel, the receptor atoms and dummy atoms options were chosen for the receptor and binding site, respectively. The ligand atoms option was selected for the target compounds. For the placement stage, the Triangle Matcher method and London dG scoring function were employed. This helped generate initial structures for the compounds within the binding pocket. The generated structures were automatically submitted for refinement. In the refinement step, the Rigid Receptor method and the GBVI/WSA dG force field were selected for final scoring and further optimization. Once all the docking elements were properly adjusted, the MDB database file containing all the target compounds was imported into the Dock Panel to initiate the docking processes. During the docking processes, each compound generated ten different poses or conformations within the binding pocket. However, only the best five poses were automatically recorded in the output file. Finally, the output files containing the docking results were examined to analyze and visualize the interactions between the protein coat and the docked ligands. This step allowed for the computation and visualization of the protein–ligand interactions, providing insights into the potential binding and interactions between the compounds and the PVY coat protein.

#### **Validation of the docking results**

Since there was no co-crystallized ligand available for the 6HXX protein, we utilized the plant virus inhibitors, ningnanmycin (NNM) and ribavirin, as control compounds. Previous molecular docking studies carried out by Abdulhassan et al. [22] and Wang et al. [35] had employed NNM and ribavirin as reference ligands to assess the activities of the investigated compounds against the tobacco mosaic virus (TMV). According to Li et al. [36], NNM is a commercially utilized plant anti-bacterial agent with anti-TMV properties. It exerts its

action by impeding the assembly of the TMV coat protein through direct interactions with specific amino acids, including Ser14, Ser15, Ser49, Trp52, Arg71, and Tyr72. To ensure consistency, the docking procedures were repeated three times following the same steps for each repetition. The docking results were analyzed to calculate the standard deviation, providing insight into the variability of the docking outcomes.

#### **In silico prediction of drug-likeness descriptors and toxicity**

To evaluate the pharmacokinetic descriptors of the investigated compounds, including their drug-likeness parameters based on Lipinski's rule of five, they were analyzed using the SwissADME website (<http://www.swissadme.ch/>). Lipinski's rule of five, proposed by Chris Lipinski and colleagues in 1997, was developed to identify molecular characteristics that may hinder permeability and absorption. According to Lipinski's rule, a molecule is considered poorly absorbed or impermeable if it violates two or more of the following criteria: (1) the number of hydrogen bond acceptors (HBA) should be  $\leq 10$ ; (2) the number of hydrogen bond donors (HBD) should be  $\leq 5$ ; (3) the molecular weight (MW) should be less than 500 Dalton; (4) the logarithm of octanol–water partition coefficient (Log P o/w) should be  $\leq 4.15$ ; and (5) the polar surface area (PSA) should be less than 140 Å<sup>2</sup> [37, 38]. In addition, the admtSAR-2.0 server (<http://lmmd.ecust.edu.cn/admtsar2>) was employed to predict the toxicity of the tested compounds using in silico assays such as carcinogenicity and AMES mutagenesis [38].

#### **Molecular dynamic simulation**

Molecular dynamics simulations were used to further study the behavior of the docked ligand–protein complexes. The simulations were conducted using the OpenMM engine and the general AMBER force field (GAFF2) on the Google Colaboratory platform [39] following the protocol described by Arantes et al. [40] with some modifications as follows:

To generate the topologies of the ligands and PVY protein coat, PDB files were loaded into the Google CoLab notebook. The systems were then prepared by setting periodic boundary boxes at 12 Å from the atoms and solvated using the TIP3P water model. Sodium chloride (NaCl) ions were added to achieve a concentration of 0.15 and neutralize the systems' charges. The solvated systems were subjected to a minimization process consisting of 20,000 steps. Subsequently, they were equilibrated for five nanoseconds with a time step of two femtoseconds under the conditions of a constant number of atoms, 1 bar of pressure, and 300 K of temperature (NPT ensemble). Snapshots were captured every ten picoseconds during the equilibration phase.

Following equilibration, molecular dynamics simulations (MDs) were performed for 100 ns under the NPT ensemble conditions, maintaining a constant pressure of 1 bar and constant temperature of 300 K. Trajectory files (.dcd files) were generated at intervals of 100 picoseconds. After the MD simulations successfully completed, the trajectories files were analyzed using the TCL scripts plugin to visual molecular dynamic (VMD) software version 1.9.3 [41]. Various properties, including root mean square deviation (RMSD), root mean square fluctuation (RMSF), radius of gyration (RoG), solvent-accessible surface area (SASA), and the number of intermolecular hydrogen bonds, were calculated from the trajectories.

## Results

### Effect of *Trichoderma* culture filtrates on the development of PVY symptoms

In terms of symptom development, the typical symptoms associated with PVY, such as mild mosaic, leaf deformation, and reduced leaf size, only appeared on untreated PVY-infected plants (Fig. 1A). In contrast, plants treated with TCFs (Fig. 1C, D, E, and F) did not exhibit symptoms. This indicates that the application of TCFs significantly suppressed the severity of PVY infection in potato plants. These findings are consistent with previous studies conducted on the culture filtrate of *T. hamatum*, which showed its effectiveness against

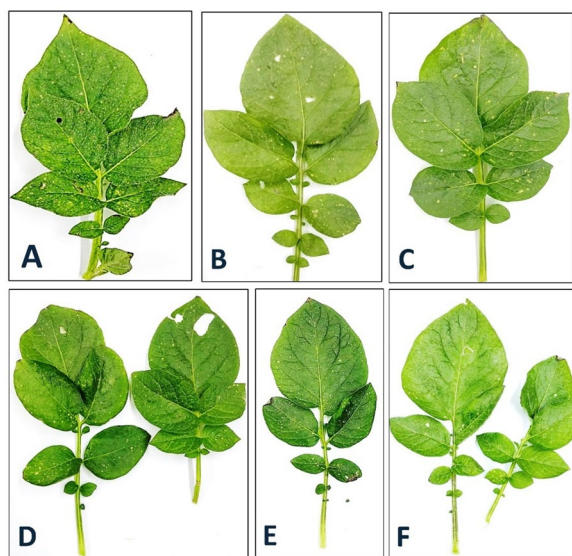


**Fig. 1** The effect of TCFs on the PVY symptoms development on potato plants at 21 days of PVY inoculation. A = infected control, B = mock control, C = treated with culture filtrate of Isolate 1, D = treated with culture filtrate of Isolate 2, E = treated with culture filtrate of Isolate 3, F = treated with culture filtrate of Isolate 4

TMV infection in tomato plants [42], and the culture filtrate of *T. viride*, which demonstrated its efficacy against PVY infection in potato plants [43].

### GC–MS analysis of *Trichoderma* cell-free culture filtrates

GC–MS was used to find out the active chemical components present in the culture filtrates of *Trichoderma* spp. (T1, T2, T3, and T4). Ninety-eight compounds were detected, exhibiting varying relative percentages ranging from 0.92 to 47.54% at different retention times (Fig. 2). Among these compounds, only 24 were found to have concentrations above 10 to 47.54% based on the GC–MS areas. Several compounds, including 9-octadecenoic acid (*Z*-), chamazulene, cyclopropanedodecanoic acid, 2-octyl-, methyl ester, linoleic acid ethyl ester, and oxiraneundecanoic acid, 3-pentyl-, methyl ester, *cis*-, were detected in all four isolates. In addition, the molecules, 4*H*-1-benzopyran-4-one, 2-(3, 4 dihydroxyphenyl)-6,8-di- $\beta$ -D-glucopyranosyl-5,7-dihydroxy-, were found in three isolates. Two isolates shared the compounds 1,2-benzenedicarboxylic acid, 12-methyl-*E*, *E*-2,13-octadecadien-1-ol, 3',8,8'-trimethoxy-3-piperidyl-2,2'-binaphthalene-1,1',4,4'-tetrone, ethanimidothioic acid, 2-(dimethylamino)-*N*-[(methylamino) carbonyl]oxy]-2-oxo-, methyl ester, sitosterol, and ethyl iso-allocholate. Furthermore, specific compounds were associated with individual isolates. Isolate No. 1 exhibited 2,6-dimethyl-*N*-(2-methyl- $\alpha$ -phenylbenzyl) aniline, cyclopropanepentanoic acid, 2-undecyl-, methyl ester, *trans*-, and 9-(2',2'-dimethylpropanoilhydrazono)-3,6-dichloro-2,7-bis-[2-(diethylamino)-ethoxy] fluorine. Isolate No. 2 contained 2(3*H*)-Furanone, 5-methyl-, cyclohexanone, 2-(4,4,4-trichlorobutyl)-, dodecanoic acid, and *N*-cyclohexyl-*N'*-(5-methyl-3-isoxazolyl) sulfamide. Isolate No. 3 was associated with oxiraneoctanoic acid, 3-octyl-, *cis*-, Tricyclo [20.8.0.0(7,16)] triacontane, 1(22),7(16)-diepoxy-, and Hexa-*t*-butylselenatrisiletane. Lastly Isolate No. 4 exhibited 1-methyl-2-pyrrolidineethanol, and 2-cyclohexylpiperidine. Detailed information about these 24 compounds is presented in Table 1.

### Molecular docking studies

#### Binding site generation of the 6HXX protein

The details of the 3D structure of PVY coat protein are presented in Table 2. Identifying the active site of the target receptor is crucial for designing effective therapeutic molecules through molecular docking investigations [38]. In this study, the binding pocket of 6HXX was identified as the largest pocket within the protein structure. The refinement and preparation of the target protein

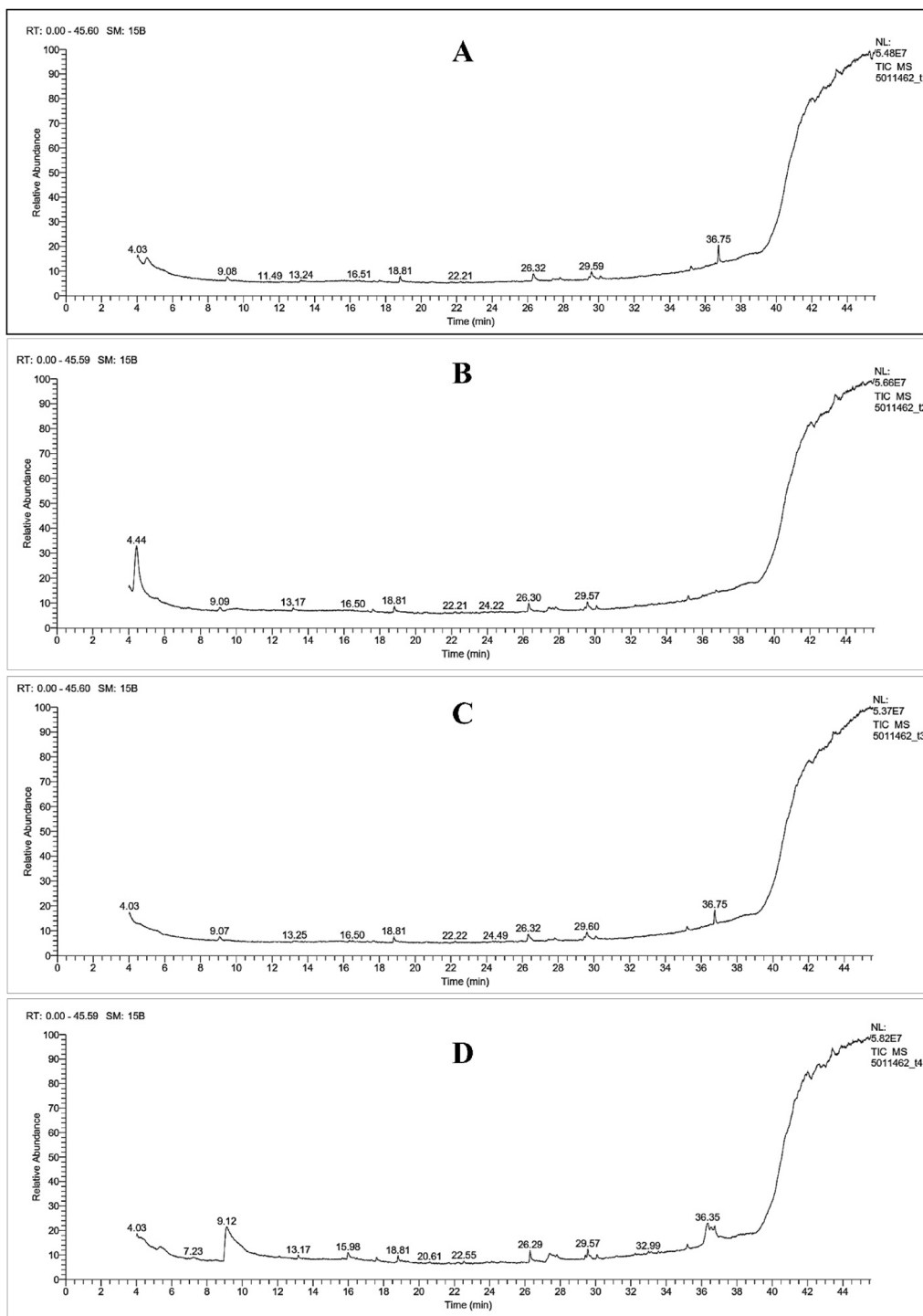


**Fig. 2** Chromatogram diagrams of GC–MS analysis of the compounds that were detected in the culture filtrates of *Trichoderma* isolates T1 (A), T2 (B), T3 (C), and T4 (D)

followed protocols described by Al-Karmalawy et al. [34], Shoala et al. [4], and Abdulhassan et al. [22]. The binding pocket contained 20 amino acids located in the central region of the coat protein gene of PVY, and they are:

Thr83, Glu121, Asn122, Gly123, Arg157, Gln158, Ala161, Arg183, Tyr184, Val187, Arg188, Asp201, Phe202, Tyr203, Glu204, His217, Met220, Lys221, Ala224, and Leu225.

**Table 1** The compounds that were detected in the culture filtrates of *Trichoderma* isolates (T1, T2, T3, and T4) with relative amounts exceeding 10% in GC-MS analysis

No	IUPAC Name	MF	MW	Trichoderma Isolates							
				T1		T2		T3		T4	
				RT	Area %	RT	Area %	RT	Area %	RT	Area %
1	1,2-Benzenedicarboxylic acid	C <sub>24</sub> H <sub>38</sub> O <sub>4</sub>	390.56	36.74	20.46	-	-	36.75	23.24	-	-
2	12-Methyl- <i>E</i> , <i>E</i> -2,13-octadecadien-1-ol	C <sub>19</sub> H <sub>36</sub> O	280.49	4.54	20.12	4.02	2.65	-	-	-	-
3	1-Methyl-2-pyrrolidoneethanol	C <sub>7</sub> H <sub>15</sub> NO	129.2	-	-	-	-	-	-	9.07	29.87
4	2(3 <i>H</i> )-Furanone, 5-methyl-	C <sub>5</sub> H <sub>6</sub> O <sub>2</sub>	98.1	-	-	4.43	47.54	-	-	-	-
5	2,6-Dimethyl- <i>N</i> -(2-methyl- $\alpha$ -phenylbenzyl) aniline	C <sub>22</sub> H <sub>23</sub> N	301.42	36.74	20.46	-	-	-	-	-	-
6	2-Cyclohexylpiperidine	C <sub>11</sub> H <sub>21</sub> N	167.29	-	-	-	-	-	-	9.07	29.87
7	3',8,8'-Trimethoxy-3-piperidyl-2,2'-binaphthalene-1,1',4,4'-tetrone	C <sub>28</sub> H <sub>25</sub> NO <sub>7</sub>	487.5	36.74	20.46	-	-	36.75	23.24	-	-
8	4 <i>H</i> -1-Benzopyran-4-one,2-(3,4-dihydroxyphenyl)-6,8-di- <i>b</i> - <i>d</i> -glucopyranosyl-5,7-dihydroxy-	C <sub>27</sub> H <sub>30</sub> O <sub>16</sub>	610.52	36.74	26.85	-	-	36.75	23.24	36.74	4.67
9	9-(2',2'-Dimethylpropanoilhydrazono)-3,6-dichloro-2,7-bis-[2-(diethylamino)-ethoxy] fluorene	C <sub>30</sub> H <sub>42</sub> C <sub>2</sub> N <sub>4</sub> O <sub>3</sub>	577.59	36.74	20.46	-	-	-	-	-	-
10	9-Octadecenoic acid (Z)-	C <sub>18</sub> H <sub>34</sub> O <sub>2</sub>	282.46	30.10	32.17	29.58	9.52	29.60	12.92	29.56	15.58
11	Chamazulene	C <sub>14</sub> H <sub>16</sub>	184.28	40.81	38.21	40.78	11.41	29.60	17.33	33.00	8.92
12	Cyclohexanone, 2-(4,4-trichlorobutyl)-	C <sub>10</sub> H <sub>15</sub> Cl <sub>3</sub> O	257.58	-	-	4.43	47.54	-	-	-	-
13	Cyclopropanedecanoic acid, 2-octyl-, methyl ester	C <sub>24</sub> H <sub>46</sub> O <sub>2</sub>	366.62	26.31	12.63	30.08	2.98	26.32	20.47	30.08	5.89
14	Cyclopropanepentanoic acid, 2-undecyl-, methyl ester, <i>trans</i> -	C <sub>20</sub> H <sub>38</sub> O <sub>2</sub>	310.51	26.31	12.63	-	-	-	-	-	-
15	Dodecanoic acid	C <sub>12</sub> H <sub>24</sub> O <sub>2</sub>	200.32	-	-	4.43	47.54	-	-	-	-
16	Ethanidithioic acid, 2-(dimethylamino)- <i>N</i> -[[[(methylamino) carbonyl] oxy]-2-oxo-, methyl ester	C <sub>7</sub> H <sub>13</sub> N <sub>3</sub> O <sub>3</sub> S	219.26	-	-	17.61	10.48	-	-	22.54	1.69
17	Linoleic acid ethyl ester	C <sub>20</sub> H <sub>36</sub> O <sub>2</sub>	308.5	40.87	3.13	40.78	8.76	40.77	10.80	29.43	2.12
18	<i>N</i> -Cyclohexyl- <i>N'</i> -(5-methyl-3-isoxazolyl) sulfamide	C <sub>10</sub> H <sub>17</sub> N <sub>3</sub> O <sub>3</sub> S	259.33	-	-	4.43	47.54	-	-	-	-
19	Oxiraneoctanoic acid, 3-octyl-, <i>cis</i> -	C <sub>18</sub> H <sub>34</sub> O <sub>3</sub>	298.46	-	-	-	-	29.60	12.92	-	-
20	Oxiraneundecanoic acid, 3-pentyl-, methyl ester, <i>cis</i> -	C <sub>19</sub> H <sub>36</sub> O <sub>3</sub>	312.49	26.31	12.63	30.08	8.74	26.32	20.47	33.00	12.13
21	Sitosterol	C <sub>29</sub> H <sub>50</sub> O	414.71	40.87	3.13	-	-	-	-	36.6	13.1
22	Tricyclo [20.8.0(7,16)] triacontane, 1(22),7(16)-diepoxy-	C <sub>30</sub> H <sub>52</sub> O <sub>2</sub>	444.73	-	-	-	-	40.77	10.80	-	-
23	Ethyl iso-allocholate	C <sub>26</sub> H <sub>44</sub> O <sub>5</sub>	436.62	-	-	40.93	3.74	-	-	40.70	12.58
24	Hexa- <i>t</i> -butylselenatrisiletane	C <sub>24</sub> H <sub>54</sub> SeSi <sub>3</sub>	505.9	-	-	-	-	36.75	23.24	-	-

RT retention time, MF molecular formula, MW molecular weight, T1 *T. asperellum* isolate Ketta, T2 *T. asperellum* isolate Ketta, T3 *Trichoderma* sp., T4 *T. asperelloides* isolate RIZK24T4

**Table 2** Details of the three-dimensional structure of the potato virus Y protein coat

PVY-CP details		3D structure of the chain of PVY-CP
Code	6HXX	
Method	Electron microscopy	
Resolution	3.40 Å	
Aggregation state	Helical array	
Reconstruction method	Helical	
Sequences length (Fig. 3)	224 amino acids	
Position	From 44 to 267	

### Molecular docking experiment

To investigate potential anti-PVY agents that target the protein coat enzyme, a molecular docking experiment was conducted. This experiment focused on the compounds identified in the culture filtrates of *Trichoderma* isolates (Table 1) through GC–MS analysis. The MOE program (version 2015.10) was utilized for the docking process. In addition, ningnanmycin and ribavirin compounds were docked at the binding pocket of the target protein, serving as reference compounds for comparison with the compounds of interest [22, 35]. For each compound, five poses were obtained through molecular docking. The best pose for each complex was selected based on docking scores, RMSD-refine value, and binding modes. The docking scores of all tested compounds ranged from  $-7.58$  to  $-3.88$  kcal/mol, with an RMSD-refine value close to 2 Å. With exception of the Hexa-*t*-butylselenatrisiletane (C24), which exhibited an RMSD-refine value greater than 3 Å. Detailed results of the molecular docking analysis for all tested compounds are presented in Table 3.

### Binding interaction analysis of the best docked compounds against the PVY coat protein

Only compounds that yielded valid molecular docking scores were selected for further investigation. The docking results revealed that seven compounds exhibited binding energies, RMSD values, and binding modes comparable to the reference ligands C25 and C26 against PVY-CP. For instance, the reference ligand C25 achieved a binding score of  $-6.50$  kcal/mol, forming five hydrogen bonds with the Asp201, Thr83, Phe202, and Lys221 residues. On the other hand, reference ligand C26 displayed an energy score of  $-5.54$  kcal/mol with three hydrogen interactions with Asp20 and Lys221 and one H- $\pi$  interaction with His217 (Table 4).

The best seven docked compounds (C7, C8, C9, C10, C13, C17, and C19) were ordered based on their docking scores from the highest (most negative) to the

lowest. Compound C13 achieved the highest score of  $-7.52$  kcal/mol, followed by C8 ( $-7.34$  kcal/mol), C19 ( $-7.03$  kcal/mol), C7 ( $-6.93$  kcal/mol), C9 ( $-6.73$  kcal/mol), C17 ( $-6.63$  kcal/mol), and C10 ( $-6.53$  kcal/mol). Detailed information regarding docking scores, RMSD-refine values, and binding interactions are represented in Table 4.

Further analysis of the docking interactions revealed specific binding patterns for each compound. For example, compound C13 formed one hydrogen bond with the Thr83 residue, while C8 formed three hydrogen bonds with His21, Lys221, and Val205 and one ionic interaction with Lys221 as well. Compound C19 established four hydrogen bonds (Arg157, Lys221, and His217) and two additional ionic bonds with Lys221. Compound C7 interacted with the amino acid Lys221 through one hydrogen interaction and one  $\pi$ -H bond. Compound C9 exhibited three hydrogen interactions (Asp201 and Thr83), and two ionic bonds (Asp201), along with one  $\pi$ -H interaction with Lys221. Compound C17 formed one hydrogen bond with Lys221, and C10 established two hydrogen bonds and two ionic interactions with Arg157. Refer to Table 4 and Fig. 3 for more details.

Furthermore, a 3D representation of the surface of subunit A of the 6HXX protein was created to visualize the positioning and fitting of the best docked compounds within the PVY coat protein's binding pocket. This visualization confirmed the stability, strong binding affinity, and the predictable activity of these compounds (Fig. 4). Interestingly, most of the tested compounds formed strong interactions with Thr83, Arg157, Asp20, His217, and Lys221 amino acids within the binding pocket of the PVY coat protein. This finding indicates that these amino acids play a vital role in the potential targeting of chemicals against the PVY protein coat.

The docking results of the investigated PVY inhibitors were compared to common plant virus inhibitors (ningnanmycin and ribavirin), provided insights into their binding modes and activities (Table 4, Figs. 3 and

**Table 3** Molecular docking scores, RMSD-refine values, and number of bonds of the 24 compounds under investigation against PVY-CP using the MOE program

C No	IUPAC name	PubChem ID	Score (Kcal/mol) <sup>a</sup>	RMSD-refine (Å) <sup>b</sup>	No. of bonds <sup>c</sup>
C1	1,2-Benzenedicarboxylic acid	8343	-7.5858±0.152 <sup>d</sup>	0.9309±0.399 <sup>d</sup>	0
C2	12-Methyl- <i>E</i> , <i>E</i> -2,13-octadecadien-1-ol	90,107,969	-6.9752±0.177	1.7559±0.272	0
C3	1-Methyl-2-pyrrolidineethanol	93,363	-4.9672±0.290	1.149±0.276	3
C4	2(3 <i>H</i> )-Furanone, 5-methyl-	11,559	-3.8876±0.042	1.7199±0.566	1
C5	2,6-Dimethyl- <i>N</i> -(2-methyl- $\alpha$ -phenylbenzyl) aniline	14,359,910	-5.9392±0.110	1.9341±0.239	0
C6	2-Cyclohexylpiperidine	92,439	-5.1546±0.000	0.9764±0.000	3
C7	3',8,8'-Trimethoxy-3-piperidyl-2,2' binaphthalene-1,1',4,4'-tetrone	590,815	-6.935±0.139	2.3228±0.660	2
C8	4 <i>H</i> -1-Benzopyran-4-one, 2-(3,4 dihydroxyphenyl)-6,8-di-b-d-glucopyranosyl-5,7-dihydroxy-	442,615	-7.3495±0.291	1.4013±0.597	4
C9	9-(2',2'-Dimethylpropanoilhydrazono)-3,6-dichloro-2,7-bis-[2-(diethylamino)-ethoxy] fluorene	590,814	-6.7325±0.262	1.9044±0.688	6
C10	9-Octadecenoic acid ( <i>Z</i> -)	445,639	-6.5393±0.261	0.8819±0.470	5
C11	Chamazulene	10,719	-4.9862±0.253	1.7836±0.577	1
C12	Cyclohexanone, 2-(4,4,4-trichlorobutyl)-	566,638	-5.3939±0.137	0.5827±1.175	1
C13	Cyclopropanedodecanoic acid, 2-octyl-, methyl ester	534,597	-7.5245±0.217	1.7788±0.454	1
C14	Cyclopropanepentanoic acid, 2-undecyl-, methyl ester, <i>trans</i> -	91,691,232	-7.1727±0.337	2.4636±0.702	0
C15	Dodecanoic acid	3893	-6.0606±0.185	1.3526±0.127	3
C16	Ethanimidothioic acid, 2-(dimethylamino)- <i>N</i> -[[[(methylamino) carbonyl] oxy]-2-oxo-, methyl ester	5,366,286	-5.582±0.241	2.0576±0.322	2
C17	Linoleic acid ethyl ester	5,282,184	-6.6359±0.324	1.2544±0.228	1
C18	<i>N</i> -Cyclohexyl- <i>N'</i> -(5-methyl-3-isoxazolyl) sulfamide	535,195	-5.9949±0.202	1.0495±0.152	1
C19	Oxiraneoctanoic acid, 3-octyl-, <i>cis</i> -	119,250	-7.0328±0.373	1.9379±0.517	6
C20	Oxiraneundecanoic acid, 3-pentyl-, methyl ester, <i>cis</i> -	71,360,559	-6.8272±0.267	1.0067±0.182	0
C21	Sitosterol	222,284	-4.8005±0.571	2.0061±0.380	0
C22	Tricyclo [20.8.0.0(7,16)] triacontane, 1(22),7(16)-diepoxy-	543,764	-5.9579±0.545	2.8108±1.196	0
C23	Ethyl iso-allocholate	6,452,096	-5.9558±0.314	2.4348±0.980	2
C24	Hexa- <i>t</i> -butylselenatrisiletane	553,169	-4.2777±0.268	5.2566±1.833	1
C25	Ningnanmycin <sup>e</sup>	44,588,235	-6.5022±0.227	1.2832±0.095	5
C26	Ribavirin <sup>e</sup>	37,542	-5.5422±0.072	0.7742±0.385	4

C No. compound number

<sup>a</sup> the score of placement of a compound into the binding pocket of the target protein using the London dG scoring function

<sup>b</sup> the root mean square deviation between the poses before refinement and those poses after refinement of the crystal structure

<sup>c</sup> the number of the bonds between the atoms of the investigated compounds and amino acids of the binding pocket of PVY coat protein

<sup>d</sup> standard deviation values, and

<sup>e</sup> reference ligands

4). Many of the compounds demonstrated excellent binding and activity, indicating good stability and high binding affinities (*i.e.*, high inhibitory capacity). Notably, compounds C8, C9, C10, C13, and C19 showed superior binding energies, RMSD values, and binding modes compared to ningnanmycin and ribavirin, suggesting their potential as promising agents for combating potato virus Y.

#### In silico prediction of drug-likeness descriptors and toxicity

In recent years, there has been a notable rise in the application of advanced techniques aimed at

reducing the time and effort required for drug discovery. One such technique involves the use of computational methods for pharmacokinetic analysis [44]. Lipinski et al. [45] have established a strong correlation between certain chemical parameters and the ADMET descriptors, such as oral absorption and partial absorption, which are influenced by low molecular weight and polar surface area (PSA), respectively. In addition, passive diffusion across lipid membranes, which is crucial for drug penetration, is facilitated by low number of hydrogen bonds and the disruption of existing hydrogen bonds. Furthermore, the efficient

**Table 4** Molecular docking scores, RMSD-refine values, and the binding interactions of the compounds that exhibited valid docking results within the binding pocket of the PVY coat protein

C No	Score <sup>a</sup> (Kcal/mol)	RMSD-refine <sup>b</sup> (Å)	Bonds between atoms of compounds and residues of PVY-CP active site					
			Ligands atoms	Receptor atoms	Receptor residues	Interaction (H-bonds)	Distance (Å)	E (kcal/mo)
C7	− 6.935 ± 0.139 <sup>c</sup>	2.3228 ± 0.660 <sup>c</sup>	O (44)	NZ	Lys221	H-acceptor	2.72	− 1.4
			6-ring	CG	Lys221	pi-H	4.31	− 0.6
C8	− 7.3495 ± 0.291	1.4013 ± 0.597	O (55)	NE2	His217	H-acceptor	3.25	− 1.1
			O (55)	NZ	Lys221	H-acceptor	2.78	− 6.6
			O (63)	N	Val205	H-acceptor	2.90	− 2.7
			O (44)	NZ	Lys221	ionic	2.89	− 5.2
C9	− 6.7325 ± 0.262	1.9044 ± 0.688	C (5)	OD2	Asp201	H-donor	3.19	− 0.9
			C (17)	OD1	Asp201	H-donor	3.12	− 1.5
			CL (59)	O	Thr83	H-donor	3.39	− 1.6
			N (8)	OD1	Asp201	ionic	3.67	− 1.3
			N (8)	OD2	Asp201	ionic	3.84	− 0.8
			5-ring	CE	Lys221	pi-H	4.05	− 0.7
C10	− 6.5393 ± 0.261	0.8819 ± 0.470	O (52)	NH1	Arg157	H-acceptor	3.04	− 4.7
			O (52)	NH2	Arg157	H-acceptor	3.07	− 2.4
			O (52)	NH1	Arg157	ionic	3.04	− 4.2
			O (52)	NH2	Arg157	ionic	3.07	− 4.0
C13	− 7.5245 ± 0.217	1.7788 ± 0.454	O (67)	OG1	Thr83	H-acceptor	3.13	− 0.7
C15	− 6.0606 ± 0.185	1.3526 ± 0.127	O (36)	NH2	Arg157	H-acceptor	3.39	− 0.8
			O (36)	NH2	Arg157 Arg188	ionic	3.39	− 2.4
			O (37)	NH2		ionic	3.16	− 3.5
C16	− 5.582 ± 0.241	2.0576 ± 0.322	N (5)	OD1	Asp201	H-donor	3.20	− 2.3
			O (13)	NH1	Arg157	H-acceptor	3.06	− 1.7
C17	− 6.6359 ± 0.324	1.2544 ± 0.228	O (50)	NZ	Lys221	H-acceptor	3.03	− 4.4
C18	− 5.9949 ± 0.202	1.0495 ± 0.152	O (14)	CE	Lys221	H-acceptor	3.47	− 0.9
C19	− 7.0328 ± 0.373	1.9379 ± 0.517	O (30)	NH2	Arg157	H-acceptor	3.41	− 0.9
			O (53)	NZ	Lys221	H-acceptor	2.95	− 5.8
			O (54)	NE2	His217	H-acceptor	3.07	− 5.6
			O (54)	NZ	Lys 221	H-acceptor	3.11	− 4.9
			O (53)	NZ	Lys221	ionic	2.95	− 4.8
			O (54)	NZ	Lys221	ionic	3.11	− 3.8
C23	− 5.9558 ± 0.314	2.4348 ± 0.980	O (62)	ND2	Asn127	H-acceptor	2.97	− 2.8
			O (70)	NH1	Arg157	H-acceptor	2.94	− 2.7
C25 <sup>d</sup>	− 6.5022 ± 0.227	1.2832 ± 0.095	C (15)	OD1	Asp201	H-donor	3.34	− 1.0
			N (46)	OG1	Thr83	H-donor	3.17	− 3.0
			O (1)	CA	Phe202	H-acceptor	3.43	− 0.6
			O (33) O (42)	CE	Lys221	H-acceptor	3.25	− 1.2
				NZ	Lys221	H-acceptor	2.90	− 4.4
C26 <sup>d</sup>	− 5.5422 ± 0.072	0.7742 ± 0.385	N (3)	OD1	Asp201	H-donor	2.99	− 5.4
			O (13)	O	Asp201	H-donor	2.95	− 1.5
			O (24)	NZ	Lys221	H-acceptor	2.97	− 3.2
			C (27)	5-ring	His217	H-pi	4.50	− 0.6

C No. compound number

<sup>a</sup> the score of placement of a compound into the binding pocket of the target protein using the London dG scoring function<sup>b</sup> the root mean square deviation between the poses before refinement and those poses after refinement of the crystal structure<sup>c</sup> standard deviation values,<sup>d</sup> reference ligands

excretion of a drug from the body necessitates a small molecular weight and a suitable log *P* value, which represents lipophilicity (the logarithm of the octanol–water partition coefficient). Evaluating the pharmacokinetic descriptors of the investigated compounds is

imperative to ensure that the compounds do not pose any lethal effects upon human consumption of crop yields [46]. The pharmacokinetic descriptors and toxicity prediction of all selected compounds (Table 4) were assessed using SwissADME and admtSAR servers, respectively. These assessments included drug-likeness

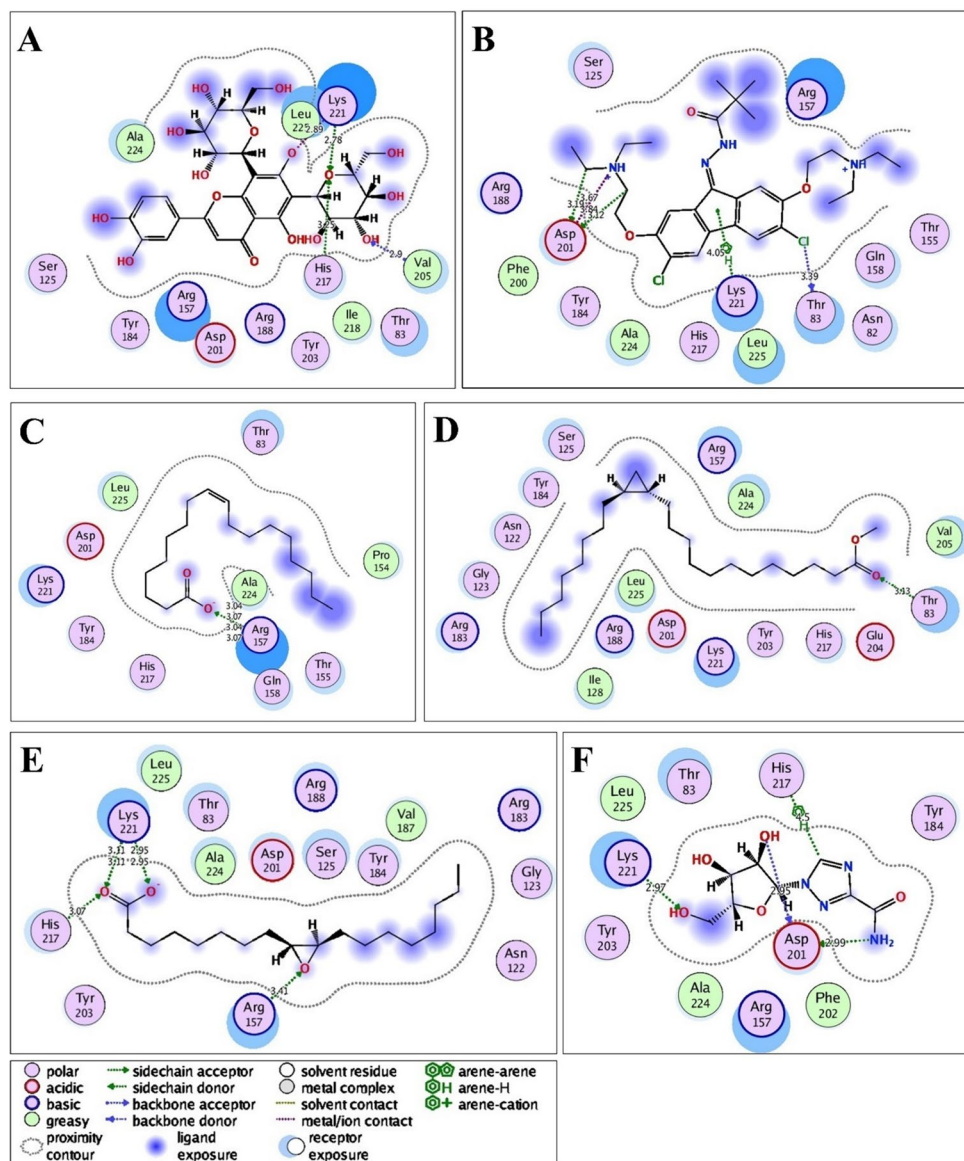


**Fig. 3** 2D molecular docking diagrams showcasing the binding interactions of the best docked compounds C8 (A), C9 (B), C10 (C), C13 (D), and C19 (E), along with the reference ligand C25 (F), within the binding pocket of the PVY protein coat

based on Lipinski's rule of five, carcinogenicity, and AMES mutagenesis. The selection criteria for suitable compounds were as follows: (1) number of Lipinski's rule violation = compounds violating two or more criteria were excluded; (2) carcinogenicity = not required; and (3) AMES mutagenesis = not present. Based on these criteria, all compounds except C7 and C8 passed for further analysis. Compound C7 violated Lipinski's rule of five and AMES test as well, while compound C8 failed to AMES test (Table 5). According to the in-silico examination of pharmacokinetic behaviors, the

tested compounds are considered safe for use with no adverse effects on humans, except for C7 and C8.

#### Molecular dynamic simulation studies

Although molecular docking is an essential method in drug design, it lacks high accuracy. So, a more precise computational technique such as molecular dynamics simulation (MDs) is needed to complement the docking studies. In general, MD simulations provide a detailed understanding of molecular behavior by applying Newton's equations of motion to calculate the motion and position of every atom within the protein-ligand

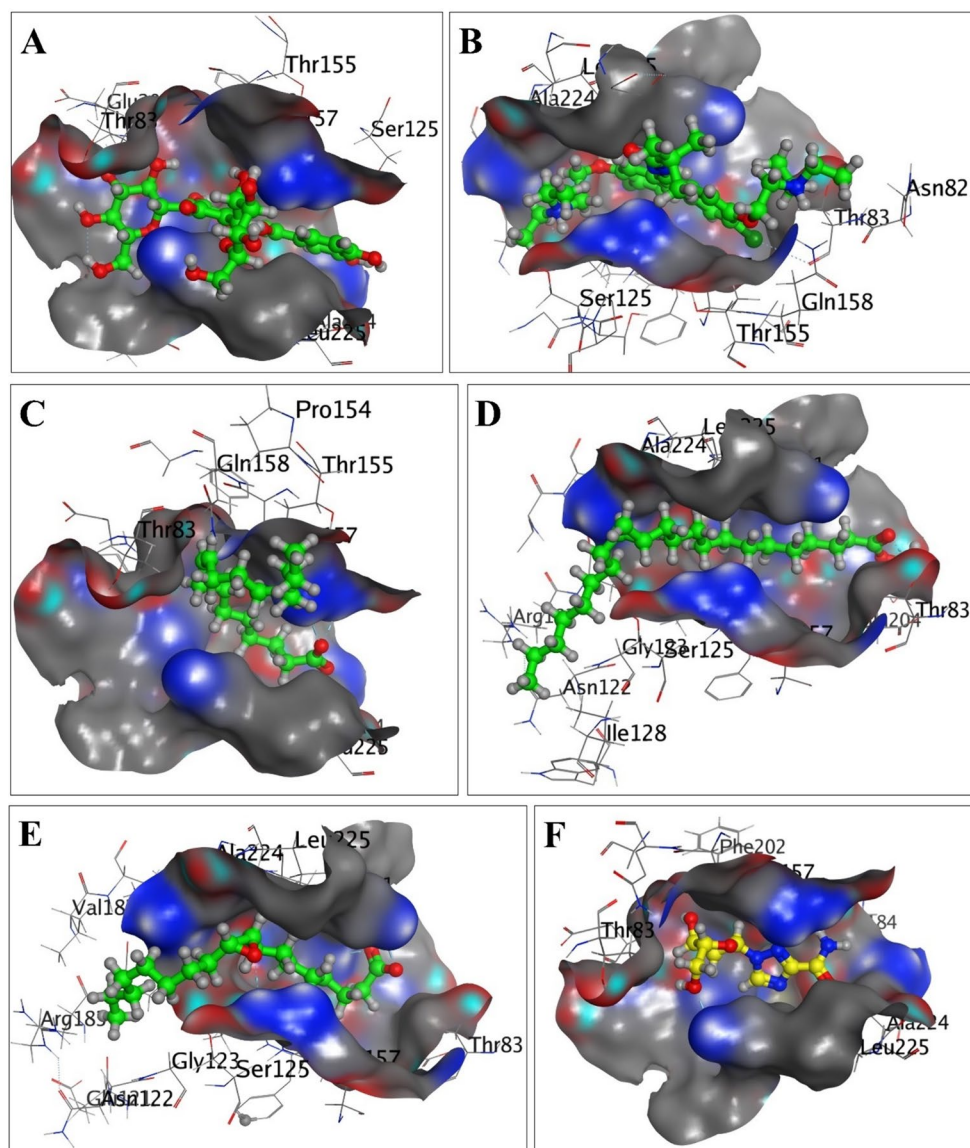


**Fig. 4** Surface of potato virus Y protein coat, depicting the positioning of the best docked compounds (represented in green as space-filling shapes), namely C8 (A), C9 (B), C10 (C), C13 (D), and C19 (E), as well as the reference ligand C25 (represented in yellow as space-filling shapes) (F)

complex over a simulation time [29]. This technique captures various essential biomolecular activities, including protein folding, conformational changes, and ligand binding, at the femtosecond timescale. The trajectories generated from MD simulations present a three-dimensional movie that depicts the system atoms' positioning at each point during the simulation [47]. Thus, MD simulations offer a more comprehensive understanding of conformational change compared to docking, resulting in a more accurate characterization of the system's behavior [29].

The final selection of the promising compounds involved two sets of criteria: (1) docking scores, RMSD-refine values, and binding modes of the reference ligands; and (2) drug-likeness properties and toxicity prediction. While most tested compounds fulfilled these criteria, the two top molecules (C13 and C19) were chosen for further analysis. These compounds were subjected to 100 ns molecular dynamic simulations to study their interactions with the *Potato virus Y* protein coat. The simulations were performed using the OpenMM package software with the general AMBER force field (GAFF2) following the protocol outlined by Arantes et al. [40].

**Table 5** Lipinski's rule of five and the toxicity predictions of the tested compounds using in silico tools

Compounds	SwissADME tools						AdmtSAR tools	
	Lipinski's rule of five						Toxicity prediction	
	MW < 500	HBA ≤ 10	HBD ≤ 5	Lipophilicity Log P ≤ 4.15	PSA < 140	Lipinski's rule violation	Carcinogenicity	AMES mutagenesis
C7	487.5	7	0	0.27	99.21	0	Non-required	Yes
C8	610.52	16	12	-4.97	291.43	5	Non-required	Yes
C9	577.59	6	1	3.87	66.4	1	Non-required	No
C10	282.46	2	1	4.57	37.3	1	Non-required	No
C13	366.62	2	0	5.61	26.3	1	Non-required	No
C15	200.32	2	1	3.15	37.3	0	Non-required	No
C16	219.26	4	1	-0.33	96.3	0	Non-required	No
C17	308.5	2	0	-0.33	26.3	0	Non-required	No
C18	259.33	5	2	1.18	92.61	0	Non-required	No
C19	298.46	3	1	3.4	49.83	0	Non-required	No
C23	436.62	5	3	3.46	86.99	0	Non-required	No

MW molecular weight, HBAH-bond acceptors, HBDH-bond donors, Log P the lipophilicity of the compounds using the MLOGP method, PSA polar surface area, AMES mutagenesis is an assay to assess the mutagenic potential of chemical compounds

The MDs trajectories were analyzed using various measures, including root mean square deviation (RMSD), root mean square fluctuation (RMSF), radius of gyration (RoG), solvent-accessible surface area (SASA) values, and the number of hydrogen bonds through simulation time to assess the stability of the systems under investigation using TCL scripts plugin to VMD software version 1.9.3 [41].

#### RMSD analysis

The root mean square deviation (RMSD) is a parameter used to assess the mean deviation of the conformational changes in protein–ligand complexes at a particular time. In general, RMSD provides valuable information about the extent of divergence exhibited by a set of atoms (such as a protein, a ligand, or a ligand–protein complex) from the original reference structure, enabling an evaluation of the system's stability [48]. High fluctuations in RMSD values indicate instability within the complex, likely resulting from conformational or orientational changes that occur during the simulation. The irregular patterns observed in RMSD values indicate unsuitable accommodations of the ligands within the binding pockets over the MD simulations timeframes [49].

In the analysis of MDs trajectories for the two studied complexes, the plots of RMSD values (Figs. 5A and 6A) demonstrate that the C13/PVY-CP complex reached a stable state after 50 ns, while the C19/PVY-CP complex achieved a stable state after 20 ns. Both complexes exhibited consistent RMSD values,

averaging around 20 Å. The RMSD values of C13 fluctuated between 3 Å and 20 Å across the first half of the simulation time and then kept equilibrium till the end of the run. Conversely, for C19, the RMSD values rapidly increased from 3 Å to 20 Å within the initial 20 ns and then remained relatively consistent till the end of the simulation run, indicating that C19 exhibited greater stability compared to C13. The significant fluctuation in RMSD values at the beginning of the MD simulations may be attributed to a new binding mode adopted by the ligand within the binding pocket [50]. The relatively steady RMSD values observed during the latter part of the simulation suggest the stabilization of the ligand's binding mode within its respective binding pocket. Based on the results obtained from RMSD analysis, both complexes achieved good stability over the MD simulations.

#### RMSF analysis

For further validation, the root mean square fluctuation (RMSF) values were calculated for C-alpha atoms of all the protein amino acids through 100 ns of MD simulations trajectories, providing insights into the mobility and flexibility of each amino acid within the protein [51, 52]. RMSF is a significant structural trait that measures the deviation of an atom or a set of atoms (e.g., protein residues) from their original positions. Higher RMSF values indicate greater divergence and structural mobility, suggesting unstable regions, while lower RMSF values indicate minimal divergence and rigidity, indicating

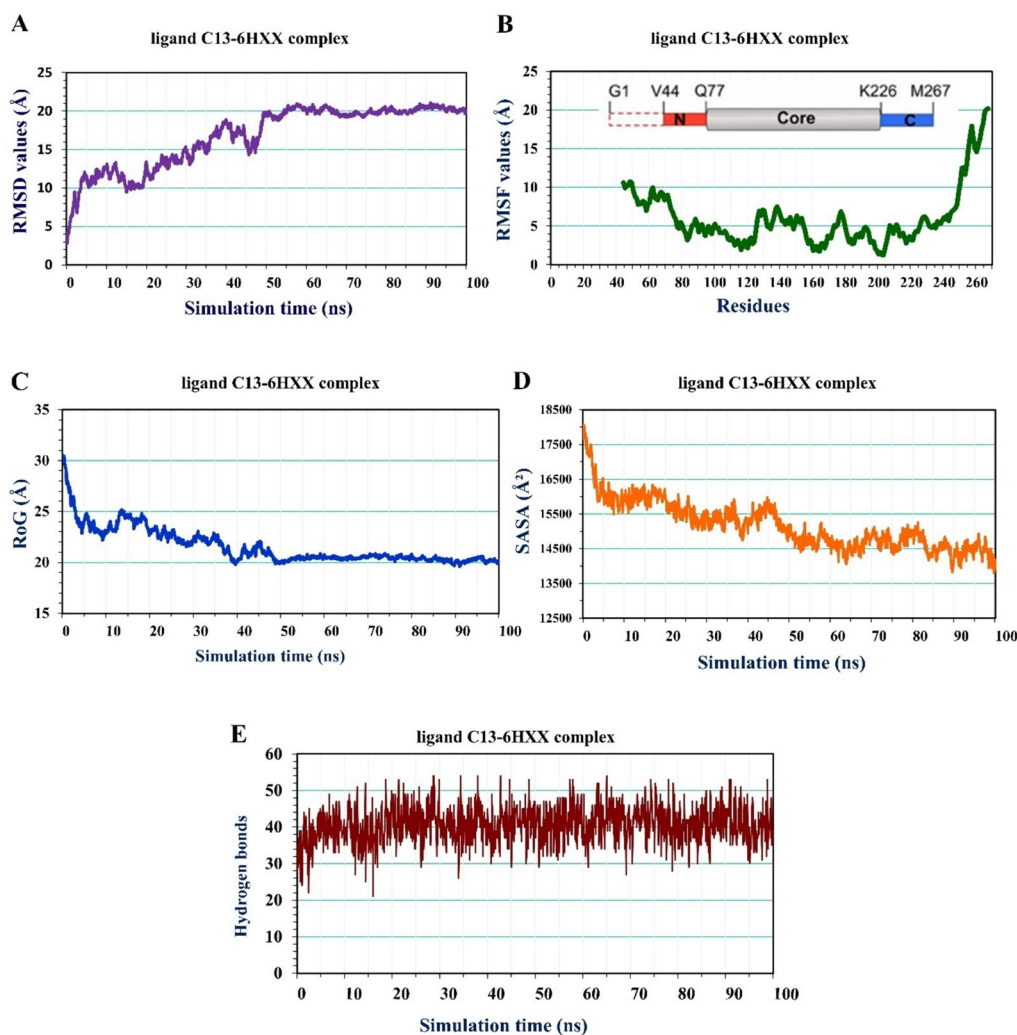


**Fig. 5** Series of plots that illustrate the analyses of the MD simulation trajectories for the ligand C13/PVY-CP complex over a duration of 100 ns. **A** The root mean square deviation (RMSD) values of the entire complex's atoms plotted against simulation time, **B** the root mean square fluctuation (RMSF) to assess the flexibility of the amino acid residues over simulation time, **C** the radius of gyration (RoG) to examine the compactness of the complex, **D** the solvent-accessible surface area (SASA) to investigate the extent of interaction between the complex and the surrounding solvent, **E** the number of hydrogen bonds formed during the MD simulation trajectories

stable regions within the system during MD simulations [51, 52].

The RMSF plot of the C13/PVY-CP complex (Fig. 5B) displays fluctuating RMSF values for amino acids in the central region (residue number 77 to residue number 226), ranging from 1 Å to 7 Å. Conversely, the RMSF plot for the C19/PVY-CP complex (Fig. 6B) exhibits relatively consistent RMSF values around the average of 2.5 Å for core region residues. The low fluctuation of amino acids in the binding site indicates slight conformational changes, suggesting that the tested ligands are strongly bound at the binding pocket of the target receptor [52]. Furthermore, the little variation in

the RMSF values of particular residues indicates their dynamic movement from the initial position due to the ligand mobility within the binding pocket during MD simulations [51]. These findings indicate that both complexes under study maintained stable binding modes throughout the simulation, with C19 exhibiting greater stability than C13 at the binding site of the PVY protein coat, consistent with the results obtained from the RMSD analysis.

It is worth noting that alpha-helical and beta-sheet regions in the secondary structure of the protein tend to be more rigid than unstructured/loop regions, resulting in lower fluctuations within these regions

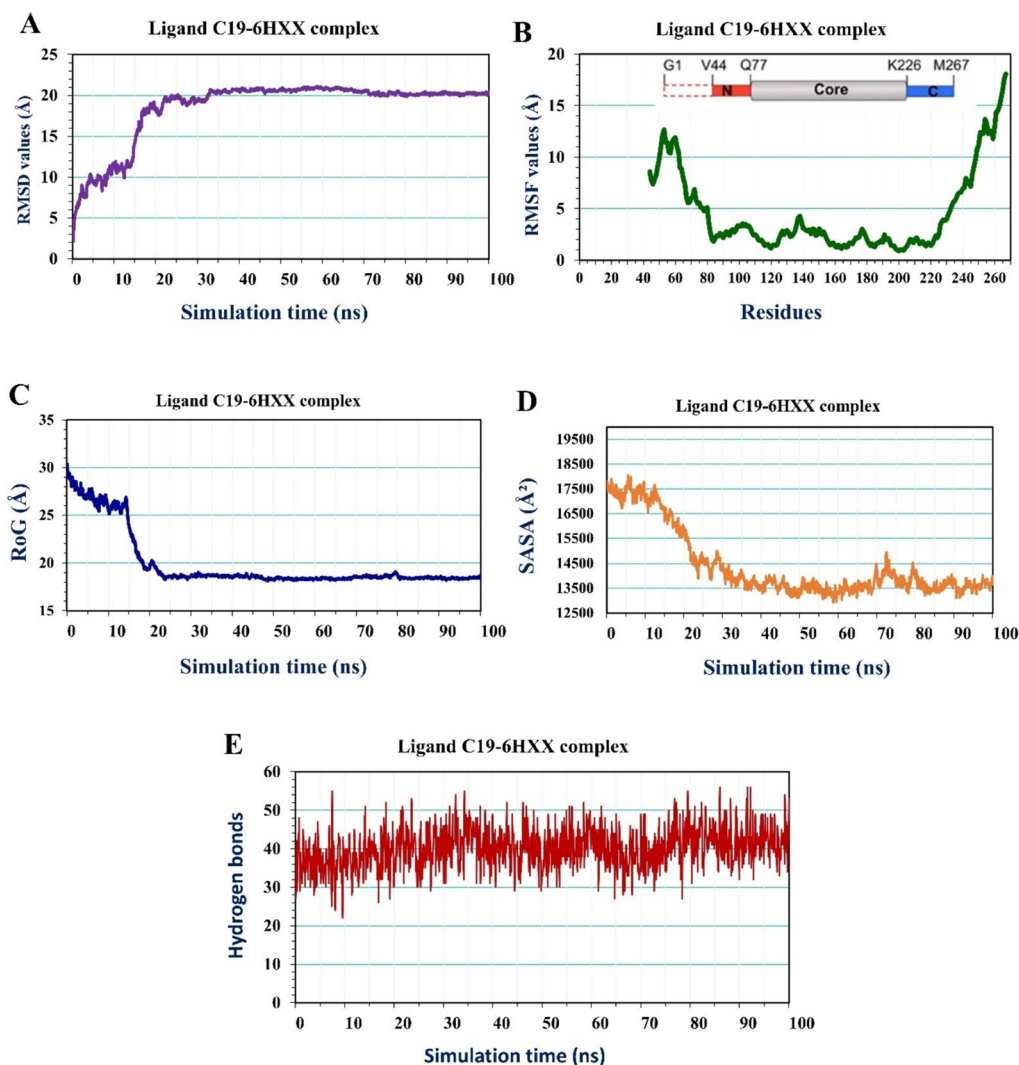


**Fig. 6** Plots displaying the analyses of MD simulation trajectories for the ligand C19/PVY-CP complex throughout 100 ns. **A** The root mean square deviation (RMSD) values for the entire complex's atoms plotted against simulation time, **B** the root mean square fluctuation (RMSF) to assess the flexibility of amino acid residues over the simulation time, **C** the radius of gyration (RoG) to examine the compactness of the complex, **D** the solvent-accessible surface area (SASA) to investigate the extent of interaction between the complex and the surrounding solvent, **E** the number of hydrogen bonds formed during the MD simulation trajectories

compared to loop regions [52, 53], which aligns with our results. Furthermore, the N-terminus (Val44 to Gln77) and C-terminus (Lys226 to Met267) regions in both complexes (Figs. 5B and 6B) exhibited more significant conformational changes compared to other regions. This behavior is attributed to the tendency of terminal amino acids to experience fluctuations due to their exposed positions [51], consistent with a previous study conducted by [52].

#### RoG analysis

To gain a better understanding about the stability of the complexes under investigation, the radius of gyration (RoG) was measured throughout the entire MD simulations trajectories. The RoG is a parameter used to determine the compactness of biomolecular structures by calculating the root mean square distance between positions of atoms and their mass center over the course of the simulation. It provides insights into the folding or unfolding behavior of the complex after the simulation and is also effective in studying the conformational

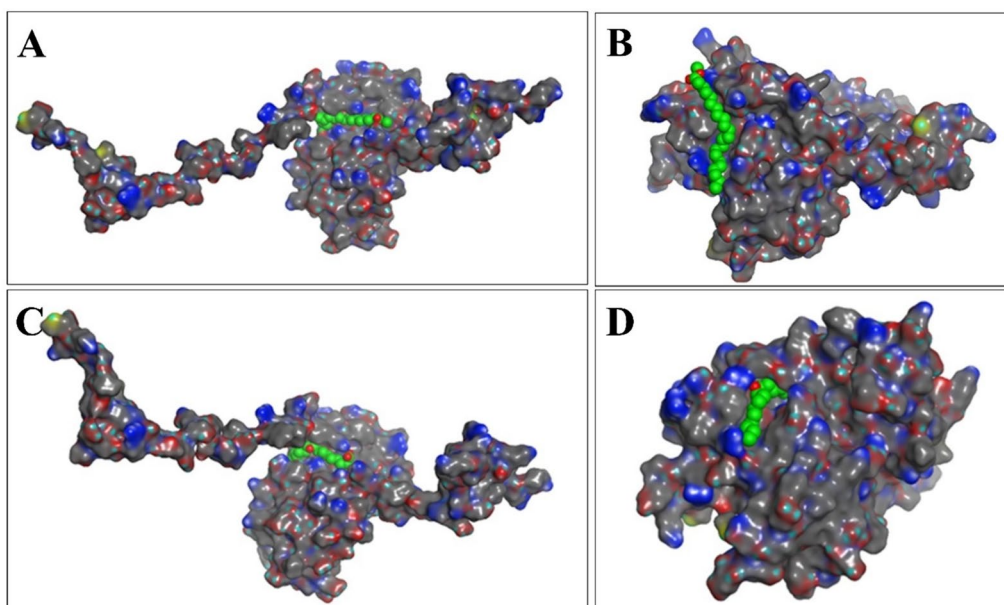


**Fig. 7** Three-dimensional positioning depicting the effect of compounds C13 and C19 on the compactness and folding of the protein during the MD simulation, **A** the C13/PVY-CP complex at the beginning of the simulation (0 ns), **B** the C13/PVY-CP complex at the end of the simulation (100 ns), **C** the C19/PVY-CP complex at 0 ns of simulation, and **D** C19/PVY-CP complex at 100 ns of simulation

changes in the 3D structure resulting from the interaction between a small molecule and a protein [38].

Consistent RoG values indicate a stably folded biomolecule, while fluctuating values suggest instability [54]. The RoG analysis of the C13/PVY-CP complex revealed that the initial RoG value was 30 Å, gradually decreasing to 20 Å after 50 ns and remaining stable around 20 Å until the end of the simulation (Fig. 5C). Similarly, for the C19/PVY-CP complex, the RoG values rapidly decreased from 30 Å to less than 20 Å within the first 20 ns and then remained consistent at around 18 Å through the remaining 80 ns of simulation (Fig. 6C). These observations indicate that the interaction of the two ligands (C13 and C19) with the protein led to a more compact and stably folded secondary structure during the simulation period (Fig. 7). This suggests strong binding of the two tested compounds to their active site throughout the MD simulation, consistent with previous studies performed by Ghasemi et al. [54], Al-Karmalawy et al. [34], and Yadav et al. [38]. Notably, C19 exhibited more favorable results than C13, aligning with the results obtained from RMSD and RMSF analyses.

#### SASA analysis

The solvent-accessible surface area (SASA) is a parameter that quantifies the surface area of a biological system complex that is exposed to a solvent. Typically measured in square angstrom (Å<sup>2</sup>), SASA represents the atoms on the surface of a biomolecule that can potentially interact

with the solvent. SASA is an essential parameter for understanding the functional structure of proteins and is commonly used in computational studies to predict the extent of conformational changes in the three-dimensional structure during MD simulations [55].

Consistent SASA values indicate a more compact and stably folded structure. The SASA plot for the C13/PVY-CP complex (Fig. 5D) reveals a decrease from 18,000 Å<sup>2</sup> to 15,500 Å<sup>2</sup> during the initial 10 ns, followed by fluctuations between 16,000 Å<sup>2</sup> and 14,500 Å<sup>2</sup> from 10 to 50 ns. Finally, the values reached equilibrium around 14,000 Å<sup>2</sup> for the remaining 50 ns of the simulation (Fig. 5D). Similarly, the SASA plot of the C19/PVY-CP complex (Fig. 6D) shows a rapid decrease from 17,500 Å<sup>2</sup> to 14,500 Å<sup>2</sup> within the first 20 ns, followed by regular fluctuations around 13,500 ns through the remaining time of the simulation (Fig. 6D). These observations indicate that both complexes achieved a relatively steady behavior and good compactness throughout the simulation time (Fig. 7). Notably, the C19/PVY-CP complex demonstrated greater stability compared to the C13/PVY-CP complex, consistent with the results obtained from RMSD, RMSE, and RoG analyses. These findings confirm the accuracy of the MD simulation procedure and the relative stability of the target protein during its interaction with the two tested compounds [56].

### Intermolecular hydrogen bonding

To further understand the behavior of the biomolecular systems at the atomic level, the number of hydrogen bonds (H-bonds) formed between the tested compounds (C13 and C19) and the PVY coat protein were calculated over simulation time. H-bonds play a crucial role as strong noncovalent interactions between the small molecules and proteins, contributing to the flexibility of protein residues and maintaining the compactness and appropriate conformation of the complex. This analysis is instrumental in understanding the stability and binding affinity of the enzyme–ligand complexes under investigation. A higher number of hydrogen bond interactions between a molecule and a protein signifies stronger binding affinity and greater stability of the complex [53, 57].

The charts of hydrogen bonds (Figs. 5E and 6E) demonstrate that the average number of intramolecular hydrogen bonds in both complexes (C13 and C19) exhibited regular fluctuations around 40 H-bonds/snapshot throughout the simulation. These findings indicate that the ligands C13 and C19 form tight bonds with the target protein over the simulation time, leading to enhanced protein's structure compactness.

### Discussion

In the current study, we focused on the coat protein enzyme of PVY as a target for combating PVY infection in potato crops. The CP of PVY is encoded by the carboxyl terminus of the polyprotein and contains 267 amino acid (aa) residues [6]. The potyviral coat protein is known as a multitasking enzyme due to its interference with all infection cycle phases. It protects the viral RNA from degradation, facilitates cell-to-cell movement, enables viral transmission by aphids, participates in virion assembly, and contributes to genome replication [10]. Unfortunately, to the best of our knowledge, there are currently no chemical agents available that provide reliable protection against PVY infection in plants. Therefore, it is crucial to urgently search for effective and environmentally friendly chemicals that target vital components of PVY, such as the capsid protein (CP).

To achieve the goal of the current study, the focus was placed on the components present in the culture filtrates of *Trichoderma* spp. The selection of these components was based on the following considerations:

Microbial metabolites emerged as promising candidates for developing effective antiviral medications due to their advantageous properties such as structural diversity, biocompatibility, and low toxicity [58]. The *Trichoderma* genus encompasses over 340 species, some of which possess the ability to defend against phytopathogens by producing a wide array of secondary metabolites,

making them valuable as biocontrol agents in agriculture [59].

*Trichoderma* species produce hundreds of secondary metabolites, including peptaibols, diketopiperazines, tetrionic acid derivatives, steroids, amides, lactones, cyclopentenones, polyketides, terpenes, pyridines, peptides, and pyranone derivatives. These metabolites exhibit various biological activities such as antibacterial, antifungal, nematocidal, antiviral, plant growth enhancement, and inducers of plant resistance [59]. The components present in the culture filtrates of *Trichoderma* isolates (T1, T2, T3, and T4) were identified using GC–MS. The analysis report of GC–MS revealed the presence of more than 90 compounds at different retention times, with concentrations ranging from 0.92 to 47.5%. To assess the bioactivities of these components against PVY using computational methods, 24 compounds with concentrations exceeding 10% were chosen.

To develop and assess the efficacy of novel antiviral compounds produced by *Trichoderma* spp. in suppressing PVY infection, *in silico* analysis methods were employed, including molecular docking, drug-likeness descriptors, toxicity prediction, and molecular dynamics simulations (MDs). Molecular docking, in combination with MD simulations, is commonly utilized to predict the binding modes, binding affinities, and stability of protein–ligand complexes. The term “molecular docking” refers to how a molecule fits itself within another molecule to evaluate its biological activities. By examining how the molecule interacts with the target protein using scoring functions, it identifies the most probable structure that occurs in nature. It is a computational process that simulates the natural linking of molecules within a cellular environment to form a stable system. Moreover, molecular docking provides the primary structure of the protein–ligand complex, which is subsequently subjected to MD simulations [20, 60].

The selected compounds were subjected to molecular docking studies using the MOE software. Prior to the docking simulation, the target protein was refined, following the methodology outlined by Yadav et al. [38]. Both the tested ligands and the target protein (ID: 6HXX) were prepared, and the binding pocket was generated. The docking runs were performed with parameters as previously described by Al-Karmalawy et al. [34], and Abdulhassan et al. [22]. To validate the docking results, ningnanmycin and ribavirin molecules were used as controls because they are commonly used as plant virus inhibitors [22, 35]. The molecular docking studies revealed that the majority of the tested compounds showed good docking scores. However, compounds such as 4*H*-1-benzopyran-4-one,2-(3,4 dihydroxyphenyl)-6,8-di-*b*-dglucopyranosyl-5,7-dihydroxy- (C8),

9-(2',2'-dimethylpropanoilhydrazono)-3,6-dichloro-2,7-bis-[2-(diethylamino)-ethoxy] fluorene (C9), 9-octadecenoic acid (*Z*)- (C10), cyclopropanedodecanoic acid, 2-octyl-, methyl ester (C13), and oxiraneoctanoic acid, 3-octyl-, *cis*- (C19) achieved superior docking scores, acceptable RMSD-refine values, and demonstrated favorable binding modes within the binding pocket when compared to ningnanmycin and ribavirin docked against the PVY capsid protein.

Notably, these compounds fitted themselves within the binding site through various interactions, including hydrogen bonds (acceptors and donors), ionic bonds, pi-H bonds, and H-pi bonds with Thr83, Arg157, Asp201, His217, and Lys221. This suggests that these amino acids play a crucial role in the potential of these chemicals to target the PVY protein coat [37]. Among these amino acids, Arg157, His217, and Lys221 are located in the alpha-helical regions at the central region of the target protein, while Asp201 and Thr83 are found in the beta strands and loop regions, respectively.

It is worth noting that the molecular docking results of the current study align with previous docking studies conducted by Hussain et al. [46] on tobacco mosaic virus (TMV), Shoala et al. [4] on potato leafroll virus (PLRV), Jeyaraj et al. [61] on chilli leaf curl virus (ChiLCV), Sangeetha et al. [11] on groundnut bud necrosis virus (GBNV), Abdulhassan et al. [22] on TMV, and Omar et al. [23] on TMV. Moreover, previous studies carried out by Abd-Alla et al. [25] and Omar et al. [23] confirmed that the docking results closely matched the experimental findings, suggesting that the compounds that achieved good stability within the binding pocket of the coat protein of PVY such as C8, C9, C10, C13, and C19 have the potential to be effective inhibitors against PVY.

The *in silico* assessment of pharmacological descriptors like drug-likeness and toxicity prediction is a critical step in the development of new medications. This assessment ensures the safety of tested molecules for humans, who would consume the treated crops by these compounds at the early stages of drug development, saving effort, time, and cost [28, 37, 38, 46]. Physicochemical properties of a molecule, including molecular weight, polar surface area, number of hydrogen bonds (acceptor and donor), and lipophilicity (log P) as per Lipinski's rule of five, are key factors in evaluating its absorption, distribution, metabolism, excretion, and toxicity (ADMET descriptors) in the body. These properties determine the efficacy and safety of the molecule [45].

All tested compounds that yielded valid docking results were subjected to evaluation using the SwissADME and admtSAR websites. These assessments aimed to determine their drug-likeness parameters according to

Lipinski's rule of five and predict their toxicity, respectively. The output results from ADMET analysis showed that all compounds listed in Table 5 can be safely used by humans with the exception of compounds C7 and C8.

Out of the compounds that successfully passed the assessment of pharmacological descriptor, the two top-performing compounds (C13 and C19) with the highest docking scores were selected for further analysis using MD simulation for duration of 100 ns. MD simulation can be seen as a computational microscope enabling researchers to visualize the behavior of the biomolecular at an atomic level [62]. Protein–ligand interactions play a crucial role in numerous biological processes. Protein can undergo conformational changes under physiological conditions, and their stability can be enhanced upon binding with a ligand [60].

Root mean square deviation (RMSD), root mean square fluctuation (RMSF), radius of gyration (RoG), solvent-accessible surface area (SASA), and the number of intermolecular hydrogen bonds were calculated from MD simulation trajectories as a function of time. For RMSD analysis, both compounds revealed relatively stable RMSD profiles after 50 ns of simulation for the C13/protein complex and after 20 ns for the C19/protein complex. This suggests that the C19 complex is more stable than the C13 complex. Analysis of RMSF plots revealed that the central region of the target protein, particularly the alpha-helical and beta-strand regions, exhibited higher stability for both systems. However, the fluctuations in the core region residues of C13 ranged from 1 Å to 7 Å, while in C19, they were around 2.5 Å. This indicates that the C19/PVY-CP complex achieved a more stable binding mode through the MD simulation run. These findings are consistent with the results obtained from molecular docking.

For a better understanding of the compactness and folding of the studied protein, the values of RoG and SASA were computed across the time of simulation. The values of RoG and SASA indicated that the C13/PVY-CP complex reached a stable state after 50 ns, while the C19/PVY-CP complex reached a stable state after 20 ns, with relatively consistent values. This suggests that both ligands influenced the conformational changes of the protein structure, leading to increased compactness and folding during the MD simulations, with C19 demonstrating superior stability. Furthermore, the number of intermolecular hydrogen bonds formed between the ligands and the target binding pocket was analyzed over the simulation time. Both complexes showed steady binding modes throughout the MD simulation run, forming an average rate of about 40 H-bonds/frame. Consistent values of RoG,

SASA, and H-bonds are considered important indicators for the stability of the system through the simulation period, indicating no unfolding process, which agrees with our findings. These results align with previous MD simulations studies performed by Al-Karmalawy et al. [34], Yadav et al. [38], Sangeetha et al. [11], Joshi et al. [55], Pan et al. [56], Zrieq et al. [52], Ouassaf et al. [51], Khan et al. [57], and Ogunyemi et al. [53], further supporting the validity of our findings.

Notably, the ligand C19 achieved the most favorable outcomes across all calculated parameters from the MD simulation trajectories, which is in line with the results obtained from the docking analysis. C19 achieved the optimal binding mode when docked into the PVY binding pocket. Although the ligand C13 showed the highest docking scores, suggesting its potential, the binding modes of C9 and C10 resembled that of C19. Moreover, these compounds (C9, C10, C13, and C19) outperformed the reference ligands in terms of docking scores, RMSD-refine, and binding modes. These results suggest that these compounds hold promise as antiviral agents for combating PVY infection. Consequently, these findings provide a solid foundation for considering the utilization of *Trichoderma* spp. culture filtrate components as antiviral agents in the pesticide market.

## Conclusion

This manuscript provides a comprehensive exploration of the antiviral potential of bioactive compounds derived from *Trichoderma* against PVY infection. Molecular docking analysis was employed to examine the binding interactions between various ligands and the target protein. Notably, C19 consistently exhibited the most favorable outcomes in terms of docking scores and binding modes, indicating a strong affinity for the target binding pocket. In addition, C9, C10, and C13 displayed similar binding modes to C19, suggesting their potential as antiviral agents.

The findings of this study suggest that *Trichoderma*-based bioactive compounds, particularly C19, show promise as effective antiviral agents for managing PVY infection. The superior performance of the tested compounds, as evidenced by docking scores and binding modes, underscores their potential as novel therapeutic candidates. In conclusion, this research has made significant advancements in the utilization of novel biologically active compounds based on *Trichoderma* and their potential applications in the field. One promising aspect is their potential for commercial formulations, which opens up new possibilities for the development of innovative products. These findings pave the way for further exploration and commercialization of *Trichoderma*-based bioactive compounds, offering promising

prospects for effective and sustainable solutions in various industries.

## Abbreviations

PVY	Potato virus Y
CF	Culture filtrates
GC–MS	Gas chromatography–mass spectrometry
ADMET	Absorption, distribution, metabolism, excretion, and toxicity
MDs	Molecular dynamics simulations
RMSD	Root mean square deviation
RMSF	Root mean square fluctuation
RoG	Radius of gyration
SASA	Solvent-accessible surface area
FAO	Food and Agriculture Organization
CP	Coat protein
ToMV	Tomato mosaic virus
AMV	Alfalfa mosaic virus
PLRV	Potato leaf roll virus
TMV	Tobacco mosaic virus
GBNV	Groundnut bud necrosis virus
PDA	Potato dextrose agar
PDB	Potato dextrose broth
SMILES	Simplified Molecular Input Line Entry System
NNM	Ningnanmycin
HBA	Hydrogen bond acceptors
HBD	Hydrogen bond donors
MW	Molecular weight
PSA	Polar surface area
VMD	Visual molecular dynamic
MOE	Molecular Operating Environment
GAFF2	General AMBER force field

## Supplementary Information

The online version contains supplementary material available at <https://doi.org/10.1186/s40538-024-00629-2>.

Additional file 1.

## Acknowledgements

We extend our thanks to the Seed Pathology and Tissue Culture Laboratory at the Faculty of Agriculture, Mansoura University, where the filtrates of *Trichoderma* isolates were prepared.

## Author contributions

Mohamed N. Rizk conducted the molecular docking, ADMT analysis, and MDs studies; Hammad A. Ketta and Yasser M. Shabana contributed to the GC–MS analysis, editing, and proofreading of the manuscript.

## Funding

Open access funding provided by The Science, Technology & Innovation Funding Authority (STDF) in cooperation with The Egyptian Knowledge Bank (EKB). Not applicable.

## Data availability

No datasets were generated or analyzed during the current study.

## Declarations

### Competing interests

There is no conflict of interest.

### Author details

<sup>1</sup>Plant Pathology Department, Faculty of Agriculture, Mansoura University, El-Mansoura 35516, Egypt. <sup>2</sup>Agricultural Botany Department, Faculty of Agriculture, Kafrelsheikh University, Kafr El-Sheikh 33516, Egypt. <sup>3</sup>National Agricultural and Food Research Council, Academy of Scientific Research and Technology, Cairo, Egypt.

Received: 7 May 2024 Accepted: 22 July 2024  
Published online: 08 August 2024

## References

- Markarov A. Causes of flowering of long-day potato species under short-day and cold-night conditions. *Russ J Plant Physiol.* 2002;49:465–9.
- Myers SS, et al. Increasing CO<sub>2</sub> threatens human nutrition. *Nature.* 2014;510(7503):139–42.
- Elsahhar S, et al. Effect of chitosan nanoparticles (CS-NPs) on in vitro regeneration response and production of potato virus Y (PVY)-Free plants of potato. *Agronomy.* 2022;12(11):2901.
- Shoala T, et al. Nanobiotechnological approaches to enhance potato resistance against potato leafroll virus (PLRV) using glycyrrhizic acid ammonium salt and salicylic acid nanoparticles. *Horticulturae.* 2021;7(10):402.
- Scholthof KB, et al. Top 10 plant viruses in molecular plant pathology. *Mol Plant Pathol.* 2011;12(9):938–54.
- Karasev AV, Gray SM. Continuous and emerging challenges of potato virus Y in potato. *Annu Rev Phytopathol.* 2013;51(1):571–86.
- Revers F, Garcia JA. Molecular biology of potyviruses. *Adv Virus Res.* 2015;92:101–99.
- Chung BY-W, et al. An overlapping essential gene in the Potyviridae. *Proc Natl Acad Sci.* 2008;105(15):5897–902.
- Seo JK, et al. The charged residues in the surface-exposed C-terminus of the Soybean mosaic virus coat protein are critical for cell-to-cell movement. *Virology.* 2013;446(1–2):95–101.
- Besong-Ndika J, et al. Cotranslational coat protein-mediated inhibition of potyviral RNA translation. *J Virol.* 2015;89(8):4237–48.
- Sangeetha B, et al. Molecular modelling of coat protein of the Groundnut bud necrosis tospovirus and its binding with Squalene as an antiviral agent: In vitro and in silico docking investigations. *Int J Biol Macromol.* 2021;189:618–34.
- Sofy AR, et al. Ameliorating the adverse effects of tomato mosaic tobamovirus infecting tomato plants in Egypt by boosting immunity in tomato plants using zinc oxide nanoparticles. *Molecules.* 2021;26(5):1337.
- Sofy AR, et al. Molecular characterization of the alfalfa mosaic virus infecting solanum melongena in Egypt and the control of its deleterious effects with melatonin and salicylic acid. *Plants.* 2021;10(3):459.
- Rizk MN, Shabana YM, Ketta HA. Chemotherapy of potato virus Y infecting potato plants using antiviral drugs. *Int J Virol.* 2021;17(1):8–19.
- Tyskiewicz R, et al. Trichoderma: The current status of its application in agriculture for the biocontrol of fungal phytopathogens and stimulation of plant growth. *Int J Mol Sci.* 2022;23(4):2329.
- Harman GE, et al. Trichoderma species—opportunistic, avirulent plant symbionts. *Nat Rev Microbiol.* 2004;2(1):43–56.
- Mohammad A, Hadi G, Masoud A. Evaluation of different combinations of *Trichoderma* species for controlling *Fusarium* rot of lentil. *Afr J Biotech.* 2011;10(14):2653–8.
- Segarra G, et al. MYB72, a node of convergence in induced systemic resistance triggered by a fungal and a bacterial beneficial microbe. *Plant Biol.* 2009;11(1):90–6.
- Luo Y, et al. Antimicrobial peptaibols induce defense responses and systemic resistance in tobacco against tobacco mosaic virus. *FEMS Microbiol Lett.* 2010;313(2):120–6.
- Raval K, Ganatra T. Basics, types and applications of molecular docking: a review. *IP Int J Compr Adv Pharmacol.* 2022;7(1):12–6.
- Meng XY, et al. Molecular docking: a powerful approach for structure-based drug discovery. *Curr Comput Aided Drug Des.* 2011;7(2):146–57.
- Abdulhassan HA, et al. In silico pesticide discovery for new anti-tobacco mosaic virus agents: reactivity, molecular docking, and molecular dynamics simulations. *Appl Sci.* 2022;12(6):2818.
- Omar AZ, et al. The curative activity of some arylidene dihydropyrimidine hydrazone against tobacco mosaic virus infestation. *J Saud Chem Soc.* 2022;26(4):101504.
- Nagalakshamma V, et al. Design, synthesis, anti-tobacco mosaic viral and molecule docking simulations of urea/thiourea derivatives of 2-(piperazine-1-yl)-pyrimidine and 1-(4-Fluoro/4-Chloro phenyl)-piperazine and 1-(4-Chloro phenyl)-piperazine—A study. *Bioorg Chem.* 2020;102:104084.
- Abd-Alla HI, et al. Investigating the potential anti-SARS-CoV-2 and anti-MERS-CoV activities of yellow necklacepod among three selected medicinal plants: extraction, isolation, identification, in vitro, modes of action, and molecular docking studies. *Metabolites.* 2022;12(11):1109.
- Ramalho TC, et al. Construction and assessment of reaction models of class I EPSP synthase: molecular docking and density functional theoretical calculations. *J Biomol Struct Dyn.* 2009;27(2):195–207.
- Chandrasekaran B, et al. Computer-aided prediction of pharmacokinetic (ADMET) properties. In: Dosage form design parameters. Amsterdam: Elsevier; 2018. p. 731–55.
- Flores-Holguin N, Frau J, Glossman-Mitnik D. In silico pharmacokinetics, ADMET study and conceptual DFT analysis of two plant cyclopeptides isolated from rosaceae as a computational peptidology approach. *Front Chem.* 2021;9:708364.
- Alnajjar R, et al. Molecular docking, molecular dynamics, and in vitro studies reveal the potential of angiotensin II receptor blockers to inhibit the COVID-19 main protease. *Heliyon.* 2020;6(12):e05641.
- Nasr-Eldin M, et al. Induction of potato systemic resistance against the potato virus Y (PVYNTN), using crude filtrates of *Streptomyces* spp. under greenhouse conditions. *Egypt J Biol Pest Control.* 2019. <https://doi.org/10.1186/s41938-019-0165-1>.
- El-Kareem MSMA, et al. Application of GC/EIMS in combination with semi-empirical calculations for identification and investigation of some volatile components in basil essential oil. *Int J Anal Mass Spectrom Chromatogr.* 2016;04(01):14–25.
- Kondapuram SK, Sarvagalla S, Coumar MS. Chapter 22—docking-based virtual screening using PyRx tool: autophagy target Vps34 as a Case Study. In: Coumar MS, editor. Molecular docking for computer-aided drug design. Cambridge: Academic Press; 2021. p. 463–77.
- Kežar A, et al. Structural basis for the multitasking nature of the potato virus Y coat protein. *Sci Adv.* 2019;5(7):eaaw3808.
- Al-Karmalawy AA, et al. Molecular docking and dynamics simulation revealed the potential inhibitory activity of ACEIs against SARS-CoV-2 targeting the hACE2 receptor. *Front Chem.* 2021;9:661230.
- Wang Y, et al. Design, synthesis, anti-TMV activity, and preliminary mechanism of cinnamic acid derivatives containing dithioacetal moiety. *Pestic Biochem Physiol.* 2020;164:115–21.
- Li X, et al. Ningnanmycin inhibits tobacco mosaic virus virulence by binding directly to its coat protein discs. *Oncotarget.* 2017;8(47):82446.
- Ismail S, et al. In silico molecular docking and pharmacokinetic studies of selected phytochemicals with estrogen and progesterone receptors as anticancer agent for breast cancer. *J Turk Chem Soc Sect A Chem.* 2018;5:1337–50.
- Yadav R, et al. Virtual screening, ADMET prediction and dynamics simulation of potential compounds targeting the main protease of SARS-CoV-2. *J Biomol Struct Dyn.* 2021;39(17):6617–32.
- Singh S, Gopi P, Pandya P. Structural aspects of formetanate hydrochloride binding with human serum albumin using spectroscopic and molecular modeling techniques. *Spectrochim Acta A Mol Biomol Spectrosc.* 2022;281:121618.
- Arantes PR, et al. Making it rain: cloud-based molecular simulations for everyone. *J Chem Inf Model.* 2021;61(10):4852–6.
- Falsafi-Zadeh S, Karimi Z, Galehdari H. VMD DisRg: new user-friendly implement for calculation distance and radius of gyration in VMD program. *Bioinformation.* 2012;8(7):341.
- Abdelkhalek A, et al. Trichoderma hamatum strain Th23 promotes tomato growth and induces systemic resistance against tobacco mosaic virus. *J Fungi.* 2022;8(3):228.
- Aseel DG, et al. Trichoderma viride isolate Tvd44 enhances potato growth and stimulates the defense system against potato Virus Y. *Horticulturae.* 2023;9(6):716.
- Tang Y, et al. New technologies in computer-aided drug design: Toward target identification and new chemical entity discovery. *Drug Discov Today Technol.* 2006;3(3):307–13.
- Lipinski CA, et al. Experimental and computational approaches to estimate solubility and permeability in drug discovery and development settings. *Adv Drug Deliv Rev.* 1997;23(1–3):3–25.
- Hussain W, et al. Penta-1,4-diene-3-one oxime derivatives strongly inhibit the replicase domain of tobacco mosaic virus: elucidation through molecular docking and density functional theory mechanistic

- computations. J Antivir Antiretrovir. 2018. <https://doi.org/10.4172/1948-5964.1000177>.
47. Hollingsworth SA, Dror RO. Molecular dynamics simulation for all. Neuron. 2018;99(6):1129–43.
  48. Schreiner W, et al. Relaxation estimation of RMSD in molecular dynamics immunosimulations. Comput Math Methods Med. 2012;2012:173521.
  49. Liu K, Watanabe E, Kokubo H. Exploring the stability of ligand binding modes to proteins by molecular dynamics simulations. J Comput Aided Mol Des. 2017;31(2):201–11.
  50. Ajmal Ali M. Molecular docking and molecular dynamics simulation of anticancer active ligand '3,5,7,3',5'-pentahydroxy-flavanonol-3-O- $\alpha$ -L-rhamnopyranoside' from Bauhinia strychnifolia Craib to the cyclin-dependent protein kinase. J King Saud Univ Sci. 2020;32(1):891–5.
  51. Ouassaf M, et al. Combined molecular docking and dynamics simulations studies of natural compounds as potent inhibitors against SARS-CoV-2 main protease. J Biomol Struct Dyn. 2022;40(21):11264–73.
  52. Zrieq R, et al. Tomatidine and patchouli alcohol as inhibitors of SARS-CoV-2 enzymes (3CLpro, PLpro and NSP15) by molecular docking and molecular dynamics simulations. Int J Mol Sci. 2021;22(19):10693.
  53. Ogunyemi OM, et al. Identification of promising multi-targeting inhibitors of obesity from Vernonia amygdalina through computational analysis. Mol Divers. 2023;27(1):1–25.
  54. Ghasemi F, et al. In silico designing of hyper-glycosylated analogs for the human coagulation factor IX. J Mol Graph Model. 2016;68:39–47.
  55. Joshi T, et al. Molecular docking and molecular dynamics simulation approach to screen natural compounds for inhibition of *Xanthomonas oryzae* pv. *Oryzae* by targeting peptide deformylase. J Biomol Struct Dyn. 2021;39(3):823–40.
  56. Pan F, et al. A molecular docking and molecular dynamics simulation study on the interaction between cyanidin-3-O-glucoside and major proteins in cow's milk. J Food Biochem. 2021;45(1): e13570.
  57. Khan S, et al. Structure-based identification of potential SARS-CoV-2 main protease inhibitors. J Biomol Struct Dyn. 2022;40(8):3595–608.
  58. Zhao L, et al. Advances and prospects in biogenic substances against plant virus: a review. Pestic Biochem Physiol. 2017;135:15–26.
  59. Li MF, Li GH, Zhang KQ. Non-volatile metabolites from *Trichoderma* spp. Metabolites. 2019;9(3):58.
  60. Naqvi AAT, et al. Advancements in docking and molecular dynamics simulations towards ligand-receptor interactions and structure-function relationships. Curr Top Med Chem. 2018;18(20):1755–68.
  61. Jeyaraj G, Mohideen HS, Geetanjali AS. Ab-initio modelling and docking evaluation of geographically derived coat proteins of chilli leaf curl virus with flavonoids and chemical compounds. J Appl Biol Biotechnol. 2021;9(1):40–51.
  62. Lazim R, Suh D, Choi S. Advances in molecular dynamics simulations and enhanced sampling methods for the study of protein systems. Int J Mol Sci. 2020;21(17):6339.

## Publisher's Note

Springer Nature remains neutral with regard to jurisdictional claims in published maps and institutional affiliations.